Digitized Theses

Digitized Special Collections

2010

Experimental analysis of the effect of porosity and primary process parameters on the cutting forces during micromilling of titanium foams

Mohammadmehdi Abolqhasemi Fakhri

Follow this and additional works at: https://ir.lib.uwo.ca/digitizedtheses

Experimental analysis of the effect of porosity and primary process parameters on the cutting forces during micromilling of titanium foams

(Spine title: Experimental analysis of titanium foams micromilling)

(Thesis format: Integrated Article)

by

Mohammadmehdi Abolghasemi Fakhri

Graduate Program in Mechanical and Materials Engineering

A thesis submitted in partial fulfillment
of the requirements for the degree of
Master of Engineering Science

The School of Graduate and Postdoctoral Studies
The University of Western Ontario
London, Ontario, Canada

THE UNIVERSITY OF WESTERN ONTARIO
School of Graduate and Postdoctoral Studies

CERTIFICATE OF EXAMINATION

Supervisor

Examiners

Dr. Remus Tutunea-Fatan

Dr. George Knopf

Joint-Supervisor

Dr. Shaun Salisbury

Dr. Evgueni Bordatchev

Dr. James Lacefield

Supervisory Committee

Dr. Ralph O. Buchal

The thesis by

Mohammadmehdi <u>Abolghasemi Fakhri</u>

entitled:

Experimental analysis of the effect of porosity and primary process parameters on the cutting forces during micromilling of titanium foams

is accepted in partial fulfillment of the
requirements for the degree of
Master of Engineering Science

Date

Chair of the Thesis Examination Board
Dr. Kamran Siddiqui

ii

Abstract

Over the recent years, porous titanium foam became a common material in biomedical applications. Since modern near-net shape technologies are still unable to achieve the desired final shape of the end product, secondary machining operations like, for instance, micromilling are currently regarded as viable manufacturing options. However, a significant lack of information exists on micromilling of porous materials. The main goal of this study was to investigate experimentally the extent of correlation between porosity and cutting forces in the context of porous titanium foam micromilling. The porosity-cutting force interplay was assessed by means of statistical metrics and the effect of several primary cutting parameters on porosity-cutting force interaction was also evaluated. A novel image-based technique was devised to determine porosity distribution along the tool path, when analyzed from a cutting kinematics perspective. Results indicate that under certain cutting conditions, good correlations exist between the signatures of porosity and cutting forces.

Keywords

Acknowledgments

Co-Authorship Statement

I hereby declare that this thesis incorporates three original papers that two have been previously submitted for publication in peer reviewed journals and to be submitted in the near future. These papers were co-authored by my supervisors, Dr. Evgueni Bordatchev and Dr. Remus Tutunea-Fatan, and the collaboration is covered in Chapters 2 to 5 of the thesis. In all cases, the key ideas, primary contributions, experimental designs, data analysis, interpretation and wrote manuscript, were of the author, and the contribution of the co-author was primarily through the provision of the research problem, reviews, supervision, and guidance throughout the project. I am aware of the University of Western Ontario policies on authorship and I certify that I have properly acknowledged the contribution of all co-authors to my thesis. I certify that, with the above qualification, this thesis, and the research to which it refers, is the product of my own work.

The papers included in this thesis are as follow,

- Chapter 2: Tutunea-Fatan OR, Abolghasemi Fakhri M, Bordatchev EV (2010) "Porosity and Cutting Forces: From Macroscale to Microscale Machining Correlations." Accepted on July 27, 2010 for publication in Proceedings of the Institution of Mechanical Engineers Part B – Journal of Engineering Manufacture.

- Chapter 3: Abolghasemi Fakhri M, Bordatchev EV, Tutunea-Fatan OR (2010) "Optical-based image analysis of porosity in micromilling of titanium foams." Manuscript no. IJAMT6353, submitted to International Journal of Advanced Manufacturing Technology.

Table of Contents

List of Tables

List of Figures

Chapter 1

1 Introduction

1.1 General

Porous metals, typically produced through powder metallurgy, represent a class of relatively new materials with wide industrial applications, lately extending into the microscale domain. Titanium foam, a class of porous metals with particular physical and mechanical properties such as light weight, high strength and full biocompatibility, is now a standard material for various dental and orthopaedic applications. In this context, Figure 1-1 depicts a dental implant prototype manufactured at National Research Council of Canada – Industrial Materials Institute.
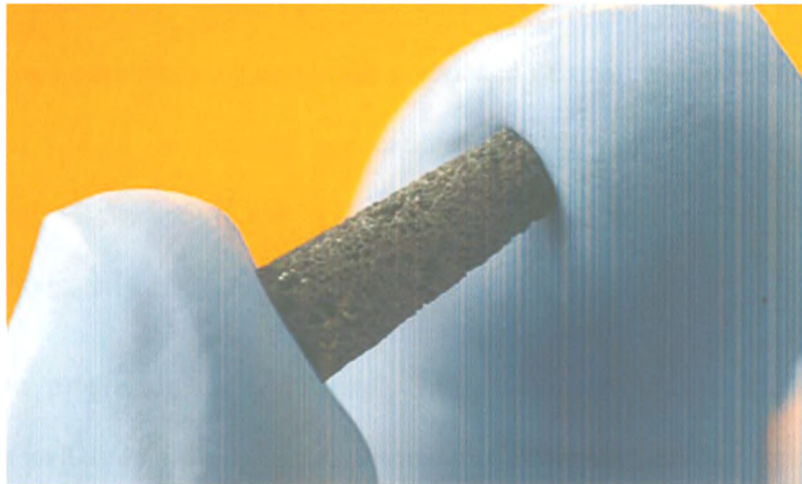
Figure 1-1: Prototype of Porous titanium foam dental implants

The porous structure of the titanium foams exhibits similarities with that of the natural bone. This promotes a superior integration of the osteoblasts within the synthetic matrix

that eventually leads to an excellent contact interface between bone and implant that is capable to transfer increased loads without the danger of loosening the implant.

Although produced in near-net shapes, most components fabricated from this material still require some form of secondary machining. In practical biomedical applications, outer surface geometry and porosity topology significantly influence the adherence between implant and neighbouring bone. New microfabrication technologies, such as micromilling and laser micromachining opened new technological possibilities for shape generation of this class of products. Besides typical geometric alterations, these manufacturing techniques enable a better control of the surface roughness that in turn affects to a large extent the friction between implant and surrounding bone tissue.

Micromilling operations, typically performed with tool sized between 100 and 400 µm, represents a good manufacturing option for production of small and precise components to be used in various engineering applications such as heat exchangers, electrical enclosures and electrodes. Figure 1-2 shows few examples of porous titanium components fabricated through micromilling.

Despite recent progresses made, relatively little is known on the inherent cutting mechanism as well as on the behavior of this material under micromilling conditions. The present work is one of the first attempts to develop knowledge on process of micromilling of porous material.
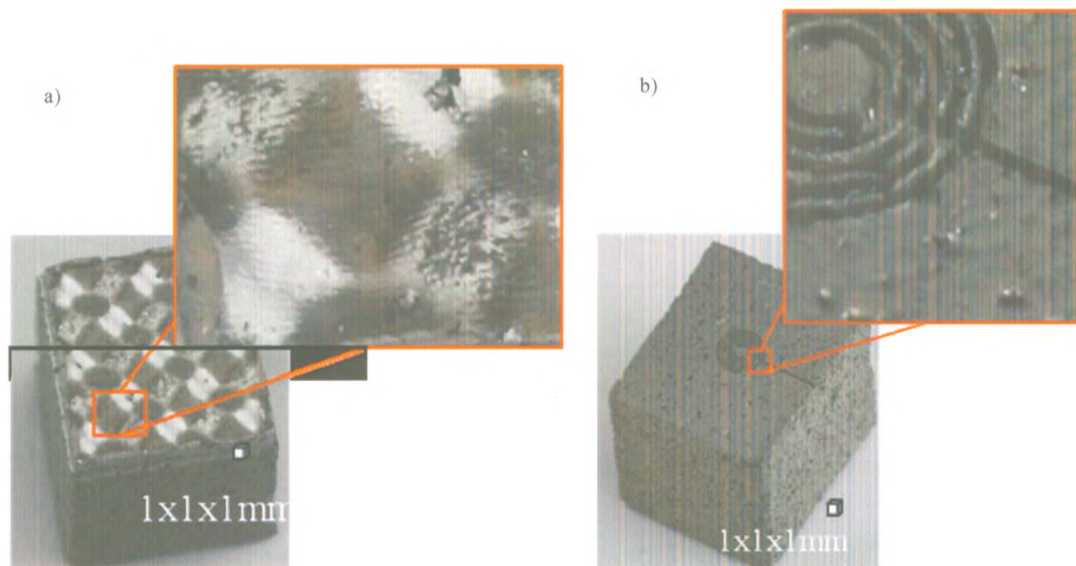
**Figure 1-2: Samples produced by micromilling process
a) freeform surface; b) circular microslot**

1.2 Contributions and Thesis Outline

The primary goal of this work is to generate knowledge on the correlation between porosity and cutting forces during porous titanium foam micromilling. While pursuing this objective, the present work will also develop understanding on the dynamics of this complex micromachining process.

Preliminary experimental observations revealed that porosity along the tool path and recorded cutting forces have a significant correlation. As it can be observed in Figure 1-3, while in solid material micromilling the amplitude of the cutting forces is quasiconstant and stable, in porous foam micromilling, cutting force amplitude experiences significant oscillations along the tool path.

The red arrows in Figure 1-3 indicate that each major variation in cutting force signature could be related to the presence of voids along the tool path.

In this work, the impact of porosity on the cutting forces as experienced during porous
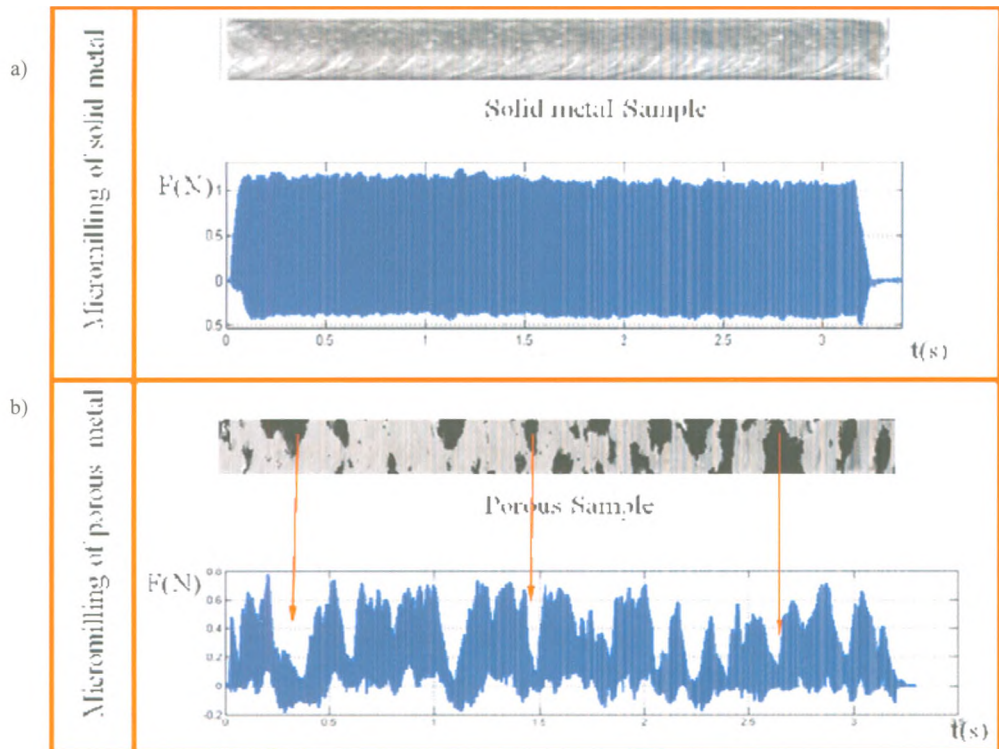
Figure 1-3: Preliminary visual correlation between cutting area geometry and cutting force in micromilling of a solid metal b) porous material

titanium foam micromilling has been examined from the perspective of the correlation between of porosity and cutting forces. Furthermore, the effect of cutting process parameters on this correlation was also investigated in order to develop practical machining knowledge. Figure 1-4 synthesizes the research scope of this thesis. All correlations studied in this work were analyzed with standard statistical metrics from signal processing theory.
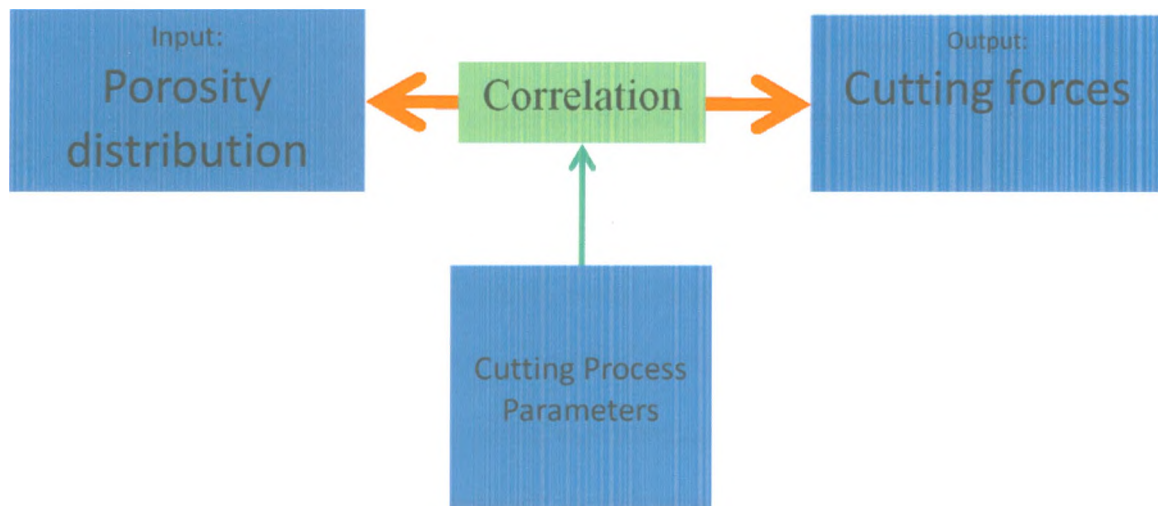
Figure 1-4: Research scope

The remainder of the thesis is structured in four chapters, out of which the first three constitute articles accepted, under review or to be submitted respectively, to various peer-reviewed journals in manufacturing. The organization of the thesis is comprised of:

Chapter 2 reviewing the main cutting theories proposed in macroscale machining, along with one of the primary parameters used to describe its machinability performances, namely cutting forces. Then, the feasibility of macroscale concepts is discussed in the context of micromachining technology that is characterized by comparable tool and pore sizes. The microslot cutting experiment performed in a porous titanium sample outlined the relative interplay between the magnitude of the cutting force and porosity of the material.

Chapter 2

2 Porosity and Cutting Forces: From Macroscale to Microscale Machining Correlations

2.1 Introduction

Porous metals are a special class of engineering materials characterized by special physical and mechanical properties like: reduced volumetric density, high surface area, increased permeability, etc. These properties strongly impact their future use since the closed porosity sought after in strong and lightweight structures could be completely undesirable in biomedical applications, for example.

Porous metals can be generated through a multitude of manufacturing processes. The most common operations used to fabricate them are: casting, deposition of metals on polymeric foams, metal powder rolling and sintering [1,2]. Generally speaking, when the initial raw material presents itself in the form of a fine and high purity metal powder, the process used to produce the metallic porous foam is denoted by the term powder metallurgy (PM). This technology has been developed mainly as a response to the need for geometrically complex components that require minor or even no subsequent machining operations, since the components generated through this process are typically characterized by a near-net shape [3].

Presently, PM is the main processing technique used in the production of porous metallic structures. The end products that can be fabricated through PM technology are extremely diverse and they range from filters, burners, pressure regulators, heat exchangers or electrical enclosures/filaments/electrodes to self-lubricating bearings, brake pads,

pneumatic mufflers, cutting tool inserts or phonic silencers. The economic impact of this technology is important since the worldwide sales of PM components worth 42 billion dollars in 2006, and half of this figure was generated in U.S. alone [4]. Due to these large numbers, PM has been acknowledged as the fastest growing metal forming technology. Traditionally, the largest market for PM was always represented by the automotive industry, but its share appears to experience a continuous decline from the 69% reported in 1998 [5]. However, this decrease was accompanied by a significant growth in other PM application areas and one of the most emerging markets for PM materials is currently represented by orthopaedic and dental implants that in most cases demand precise micromachined features [6-8]. Although it is rather difficult to estimate at this time to what proportion the porous materials have already replaced their continuous equivalents, the potential of growth estimated for these markets is considerable: $14 billion for orthopaedic biomaterials in 2002, with an expected growth rate of 7% to 9% annually [9] while the worldwide dental implant market is estimated to reach $3.5 billion by 2010 [10].

Fabrication of PM materials typically consists of three main steps: powder fractioning and preparation, compaction or molding, and sintering [11]. The compaction performed before sintering aims to increase the strength of the green part by cold welding of the particles in their common contact areas, which increases overall strength and density of products after the sintering process [12]. The physical and mechanical properties of the porous PM materials are strongly dependent on the type of raw metal powder used and on the parameters of the sintering process. The four most common porous PM materials are bronze, stainless steel, nickel and nickel based alloys. However, in newer applications,

many other materials such as titanium, aluminum, copper, platinum, gold, silver, iron, iron aluminide, niobium, tantalum and zirconium are fabricated into porous materials from powder [13]. Moreover, by changing sintering parameters, different material porosities can be achieved. The typical density for sintered PM materials ranges between 25 and 80% from the theoretical mean density of the continuous material, but it can reach 85 – 90% level in case of structural PM materials [14]. After sintering, secondary operations are widely used on PM parts to improve their density, strength, shape, tolerances and corrosion resistance. Although completely undesirable from a financial perspective [15], secondary operations are typically added to the manufacturing process to enhance the roundness, flatness and other dimensional tolerances that cannot be stabilized appropriately during sintering [14].

The objective of the present study is to review the main cutting theories and performance parameters that have been used so far in macroscale machining of the porous sintered metals in an attempt to identify any valuable knowledge to be transferred into the microscale domain. Since the lack of studies focused on micromachining operations involving porous metallic materials is almost absolute, a microslot cutting test was devised and performed on cubical samples of a porous titanium-based alloy that was manufactured through a patented procedure [16] primarily for biomedical applications (Figure 2-1). During micromachining operations, the magnitude of the cutting forces was recorded in order to demonstrate their interplay with distribution of the porosity within the material. Based on the experimental results acquired, preliminary conclusions as well as future research directions will be presented.

Figure 2-1: Porous titanium sample.

2.2 Macroscale Machining of Metallic PM Materials

By definition, near-net shape technology aims to produce parts as close as possible to their final shape and contour. As a result, the finished products generated according to this manufacturing principle will always require a minimum amount of cutting that supposed to be inexistent in an ideal situation [17]. Powder metallurgy being one of the traditional near-net shape manufacturing processes, a discussion about machining in this context might appear at first as a relative paradox. However, a more in-depth analysis reveals that common industrial practice requires that large fractions of PM parts to be subjected to finish-machining before final assembly [5]. While in the past it was estimated that approximately 30% of the PM structural components produced for the automotive industry involve at least some form of machining [18], more recent studies indicate that nearly half of the PM components require secondary machining operations

[19]. Among them, drilling, turning, milling and boring are typically used to bring the part to its final shape since dimensional stability and surface finish of the sintered PM components is relatively difficult to control through primary forming technology used to produce them. In addition to this, numerous threads and holes in the PM components are defined by axes that are either inclined with respect of the main pressing axis or involve some degree of undercut and therefore they can only be fabricated through machining.

2.2.1 Material Removal Theories

2.2.1.1 Interrupted Cutting Theory

Numerous studies have attempted to use interrupted cutting theory to explain the cause of poor machinability observed in porous sintered metals when compared to their continuous equivalents [20,21]. According to this theory, machining of the porous metals could be assimilated with an interrupted cut, caused by an intermittent engagement with workpiece material and pores, respectively. For variable periods of time, the cutting edges are either fully engaged or fully disengaged in the machining action, depending on their relative position within the structure of the material (Figure 2-2). The cutting loads have a cyclic nature, however their periodicity varies since it is primarily controlled by the random succession of continuous material and voids within the PM material [22].
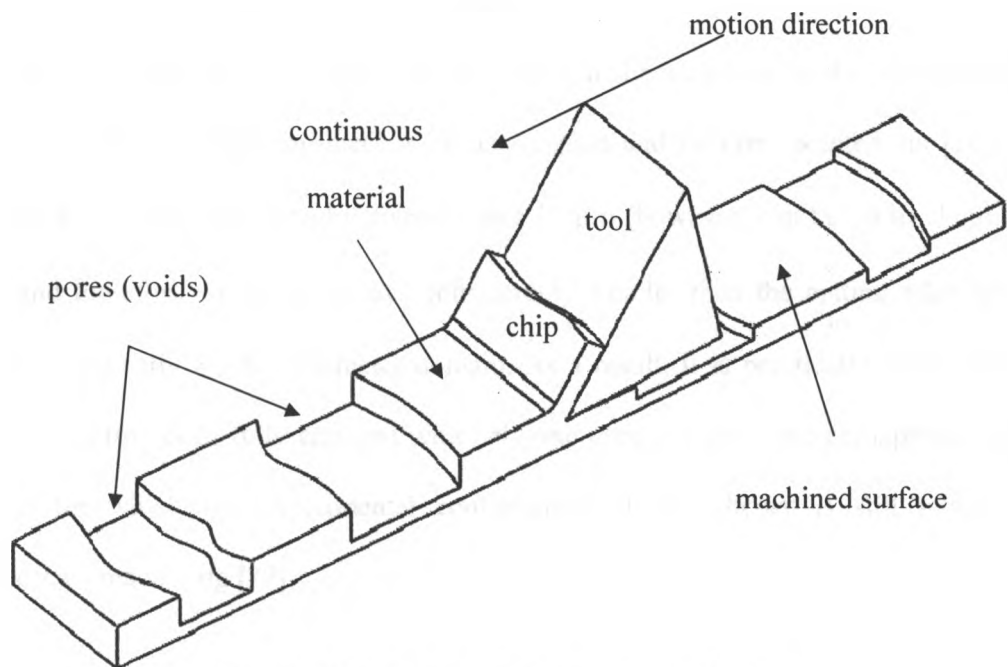
Figure 2-2: Interrupted cutting mechanism.

The frequent loading-unloading cycle exerted on the cutting edges is deemed responsible for thermal and mechanical fatigue loads exerted on the tools that eventually favour an accelerated microcrack development within their structure. The rapid microcrack growth represents the cause of premature tool wear translated into an extremely limited tool life [23]. Moreover, the discontinuous nature of the contact between the tool and workpiece increases the dynamic localized stress on the cutting edges and accelerates the negative effects of the tool chatter and undesired vibrations that ultimately lead to poor machinability indices that are characteristic of PM materials [24,25].

Based on this theoretical model, some authors [22,26] have attempted to explain the accelerated tool wear as a consequence of the large surface area introduced by the porosity of sintered material that would in fact increase the probability of physical and chemical reactions between tool and workpiece. By contrast, other studies tend to

13

postulate that the contact area between the tool and workpiece is always the same, regardless the presence or absence of the voids in the structure of the material [27]. Regardless of the underlying mechanics, as Agapiou and DeVries pointed out [28], the average pore is typically sized between 1 and 10 μm (however, can be up to about 100 μm) and therefore would be always considerably smaller than the cutting edge whose length is typically in the millimeter domain. As a result, it is practically impossible to have the cutting edge fully engaged with only one pore at a time and perhaps this is the reason for which the experimental confirmation of this theory is still lacking in macroscale machining [29].

2.2.1.2   Deformation Cutting Theory

One of the consequences of the machining operations performed on continuous metals is formation of a superficial work hardened layer. This thin layer, whose microhardness is considerably higher than that of the material, is generated by the high deformation and high stress state induced by the mechanical action of the cutting tool on the surface of the workpiece. When porous sintered metals are machined, an increase in the density of the superficial layer is also noticeable [30] and therefore it was hypothesised that workpiece material is subjected to the same high plastic deformation state that was observed while cutting continuous materials [29].

According to this theory, the permanent pressure exerted by the cutting edge on the porous material pushes its particles into the adjacent vacant pores (Figure 2-3a) and a layer of quasi-continuous material that contains little or no porosity forms on top of the machined surface (Figure 2-3b). Although removal of the porous material through

shearing followed by mechanical separation is still present, it is reasonable to believe a significant percentage of the energy consumed during machining is spent on bending and transport of the material that eventually fills the pores. As porosity increases, the depth of the compacted layer also increases, but its microhardness decreases and therefore a lower cutting force will be required to remove the material, an observation that is consistent with some of the experimental data acquired while drilling stainless steel [28,31]. However, lower cutting forces should also mean longer tool life – especially when cutting materials characterized by high porosities – and this contradicts some of the prior experimental measurements [21] as well as the low machinability index that is typically associated with metallic porous foams [32,33].

Despite the relative discrepancies between theory and experiments, the deformation cutting model explains more adequately the porosity closure phenomenon whose occurrence was consistently reported while performing turning or milling operations on metallic porous materials that were either titanium or tantalum-based [34-40]. In most cases, porosity closure or "surface smearing" can be recognised visually without difficulty as a post-machining effect (Figure 2-4). Depending on the application, surface smearing can be perceived either as a positive or as a negative consequence of machining. For example, while a controlled porosity closure could guide the flow through a filter in a desired direction by means of copper infiltration and polymer/resin impregnation [14,22], a reduction with 40% of surface pores will prevent to a high degree an efficient osteointegration between the bone and implant [40]. Although porosity losses caused by densification of the superficial layer can be eliminated – at least to a certain

extent – through controlled chemical etching [14,41], this procedure is generally regarded as risky due to possible contamination hazards.

a)

b)
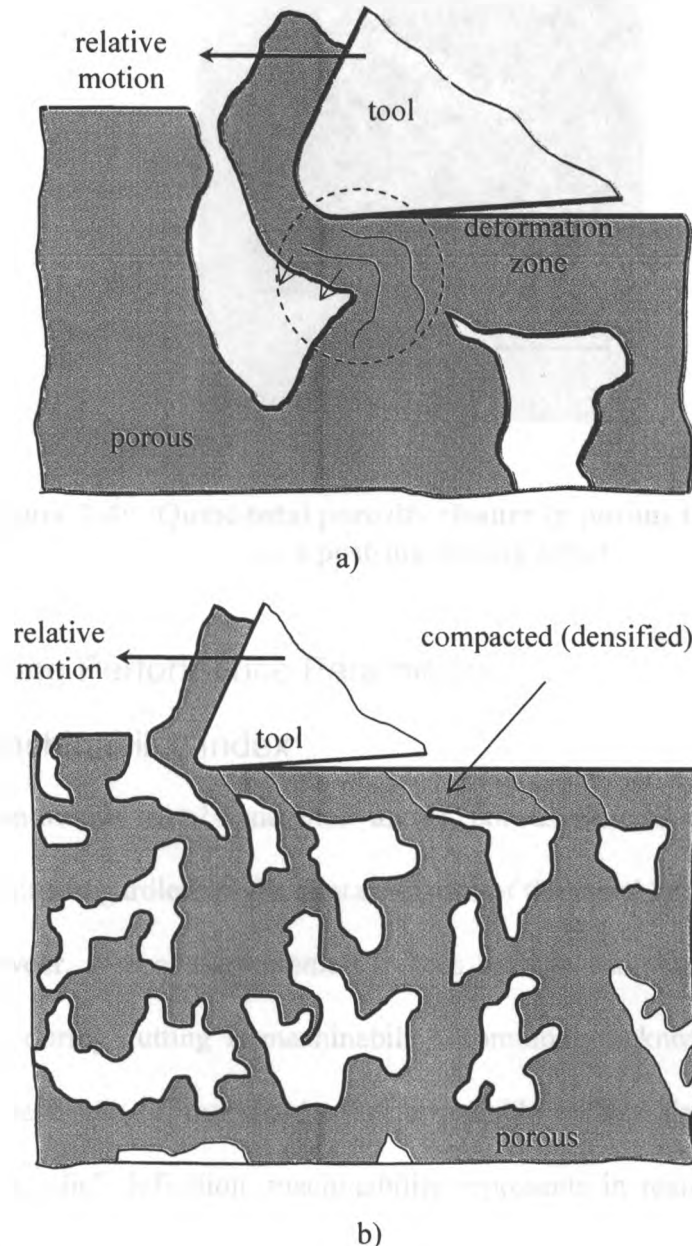
Figure 2-3: Deformation cutting mechanism: a) continuous pressure exerted by the tool leads to pore closures through permanent deformations of the workpiece material;   b) formation of the densified layer at the surface of the machined part.

Figure 2-4: Quasi-total porosity closure in porous titanium as a post-machining effect.

2.2.2 Cutting Performance Parameters

2.2.2.1 Machinability Index

Unlike most continuous metals and their alloys, porous sintered metals are generally difficult to machine, regardless of the characteristics of the metal or alloy constituting the base of the powder. One of the common indices used to estimate the behaviour of a certain material during cutting is machinability, commonly acknowledged as the ease with which a metal can be machined to an acceptable surface finish. In spite of this simple "non-scientific" definition, machinability represents in reality a fairly complex measure that does not express a physical property of the material, but rather how the material behaves under certain cutting conditions [42]. Historically, numerous definitions of the machinability have been proposed both for continuous and PM materials

[5,23,24,26,28] but the fact no standardized definition exists today proves once more the inherent complexity of the concept [43].

A comprehensive study on machinability of the PM steels has been recently published by Salak et al. [29] and it was later reviewed by Alizadeh [19]. In these works, the authors advocate for the existence of factors that either decrease or increase the machinability of sintered steels. According to this classification, the first category would include factors like: the purity of the powder and mixture components, the technological accuracy of the processing methods, the influence of the alloying elements and the amount, morphology and/or distribution of the porosity. On the other hand, the negative consequences of the aforementioned factors on the machinability can be counteracted to some extent by the positive effects of machining additives like MnS or MnS and BN that are able to simultaneously reduce the cutting forces and to allow a better chip removal. Another option that could be used to enhance the machinability of the porous sintered metals involves their cutting in a "green" or pre-sintered state [36,44] followed by secondary sintering operations. In addition to superior corrosion resistance and better surface preparation for subsequent coating operations, intentional porosity seal-off through polymer/resin impregnation was also reported to have beneficial effects on machinability of porous metals [45], which might be regarded as an advocate in favour of interrupted cutting theory.

However, the debate on prevalence of one or the other material removal mechanisms in machining of porous metals is still ongoing, since the two cutting theories detailed in Section 2.2.1 seem to propose conflicting answers when it comes to establishing a correlation between porosity and machinability. While interrupted cutting theory

postulates that a lower porosity will improve machinability, deformation cutting theory predicts exactly the opposite. On the other hand, deformation cutting theory is better supported by experimental and practical observations and perhaps this is the reason some researchers believe that the influence of the microstructure should be more carefully considered when investigating machining operations performed on porous metals [29].

In order to quantify the machinability of the porous sintered metals, prior studies relied on a number of measurable machining parameters: temperature in the cutting area, cutting forces, surface finish, tool wear, etc. Similar to continuous machining, these parameters are strongly influenced by the combination of materials involved in the tool/workpiece pair as well as by the tool geometry, but the amount of porosity also plays an important role. While various types of dependencies link all the aforementioned machinability parameters to porosity, probably the most important one from the perspective of tool/workpiece interaction dynamics is represented by cutting forces.

2.2.2.2   Cutting Force

Regardless if machining continuous or porous materials, cutting forces remain one of the most common parameters used to characterize the performance of the process. The relative simplicity of the experimental procedure required to acquire their magnitudes, combined with their strong interdependence with numerous other significant machining parameters makes cutting forces extremely useful in gaining valuable insights on the mechanics of cutting. As a result, there is no surprise that a number of papers focused on machining of the metallic porous foams have reported cutting force measurements [28,31,35,37,46-49]. However, the large majority of these studies were interested in using

the cutting forces merely as a measure of the impact of various factors (porosity, additives, tool materials, etc.) on the machinability of the porous sintered metals.

As pointed out by Armarego et al. [50], only a very small proportion of the published research on PM materials has been directed towards investigation of the machining processes performed on porous sintered metals. As a result, an extremely limited number of authors have tried to propose theoretical cutting force models specifically intended for these materials. The vast majority of the models identified in the literature proposed empirical formulations of the cutting force components in turning operations in an attempt to establish a relationship between their levels and the amount of porosity and/or machinability index of the investigated material [49,51-53]. The only exception from this pattern seems to be the predictive model of the cutting force specifically developed for porous sintered metallic materials by Armarego et al. [50] that reinforced once more the idea that most determinant characteristics of the macroscale machining process (chip formation, cutting parameters, mechanics of cutting) are very similar in their inherent nature, regardless if cutting porous or continuous metals.

2.3 Cutting Forces in Micromachining of Metallic PM Materials

The increasing demand for miniaturized components and devices has generated an equally increased interest towards manufacturing technologies that are able to produce them on large scales. Among them, micromachining was always regarded as one of the best options due to its productivity, precision, surface complexity as well as applicability to a wide variety of materials [54]. The distinctive features of the micromachining process have constituted the object of an intense research activity that was reviewed by

few papers on this topic [54-57]. According to them, the number of challenges encountered in modelling of the micromachining forces is considerably larger when compared to their macroscale equivalent. These new challenges are mainly introduced by the limitations of the experimental equipment used to acquire the cutting forces, the impact of a relatively large cutting edge radius or minimum chip thickness on the dynamics of cutting as well as fragility of the tool.

In spite of the considerable body of work dedicated to micromachining, most cutting force models proposed in the past are applicable to continuous materials only, since very little research on this topic was carried out on porous metals. Nevertheless, it is important to recognize that real time monitoring and/or prediction of the cutting forces is able to offer extremely valuable information on integrity and durability of the tool used in micromachining operations performed on porous metals.

One of the few attempts identified in this direction emphasized once more the importance of the microstructure on the overall performance of the micromilling process [58]. The experiments, performed on tungsten-copper sintered composite materials, revealed that homogeneity of the microstructure and size of the particles strongly influence the machinability of the porous material. Moreover, Vogler et al. [59] have proposed a mechanistic model in micromilling that was explicitly developed for multiphase materials. Their model showed that the microstructure of heterogeneous materials can account for more than 35% of the energy of the cutting force signal and also that the frequency of variation of the cutting force is correlated with distribution of the secondary phase, while its sizing determines the magnitude of the variation. Further improvements brought to this model [60,61] revealed that surface roughness obtained after micromilling

operations performed on multiphase ductile iron materials is a combination of geometric, minimum chip thickness and burr formation effects. The burrs formed at the grain boundaries were considered a consequence of an interrupted chip-formation effect. As it will be shown in the next section, the correlation between cutting force and size/distribution of the secondary phase can be replicated in case of porous metals by simply assuming that the secondary phase it has been replaced by voids.

2.4   Micromilling Case Study

2.4.1   Workpiece Material

In order to outline the presence of the correlation between porosity and cutting force, a series of experiments were performed on Ti-6Al-4V foams manufactured through a patented powder metallurgy process [15]. A synthesis of the structural and mechanical properties of the metallic porous material is presented in Table 1. The samples were produced in cubic shapes with an average side size of approximately 13.5 mm (Figure 2-1). The material exhibits good biocompatibility and osteointegration properties [5] as a direct consequence of its highly interconnected porous structure (Figure 2-5).

Table 2-1:   Structural and mechanical properties of Ti foams

Property	Value
Porosity	54 %
Pore size	50 – 1400 µm
Yield strength	115 MPa
Compressive elastic modulus	10 GPa
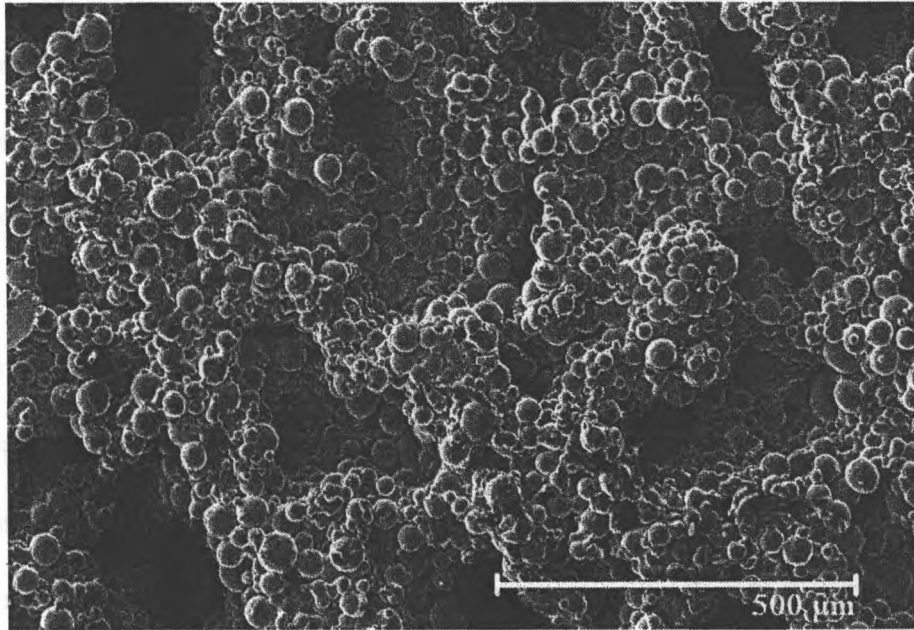
Figure 2-5: SEM microphotographs outlining microstructural characteristics of the porous titanium.

2.4.2   Experimental Setup

Micromachining experiments were carried out on a custom-built five-axis CNC micromilling machine equipped with an air-bearing spindle capable of rotational speeds between 5,000 and 100,000 RPM range (Figure 2-6). The machine is able to ensure a static positional accuracy of 0.1 µm over a 300 mm maximum travel range. Cutting forces magnitudes were acquired on X, Y and Z-axes with a Kistler 9256C2 dynamometer characterized by a high eigenfrequency value ranging between 4 and 4.8 KHz and a mimimum cutting force threshold of 0.002 N. The charge signals were converted to voltage signals with a Kistler dual mode charge amplifier type 5010B and then fed for recording purposes to a computer equipped with a National Instruments PCI-6602 data acquisition card running a real-time operating system.

Cutting forces were acquired while performing a series of conventional microslot cutting experiments with a flat end micromill. The microslots were cut with a two-flute uncoated tungsten carbide (WC) flat end micromill of $D = 800$ μm diameter with helix and clearance angles of 25° and 6°, respectively (Figure 2-7). SEM measurements yielded an approximate value of 0.95 μm for cutting edge radius. The microslots were cut on the top face of the cubic specimen and they were surrounded by a network of deeper transversal and contour grooves that were machined in advance to ensure the dimensional stability of the microslot cutting process (Figure 2-8a). The microslots (Figure 2-8b) were $d = 40$ μm deep and $l = 4$ mm long with a width corresponding to the tool size $w = D = 800$ μm. The transversal grooves were large enough to allow a complete disengagement of the tool from the current microslot without engaging the next adjacent patch ($w_g > D$).
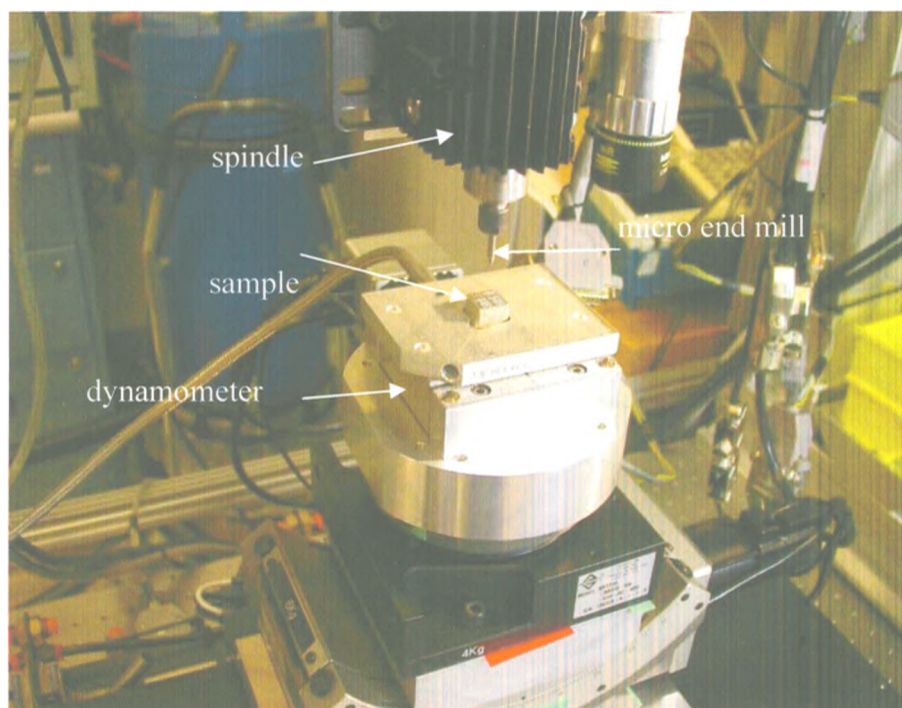
Figure 2-6: **Experimental setup used in cutting force measurements**
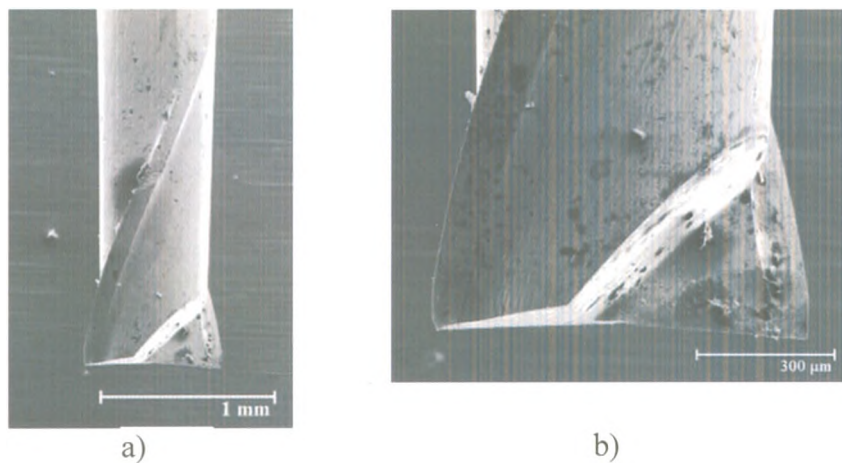
Figure 2-7: SEM picture of the two-flute micro end mill:
a) overview; and b) detail view of the tip geometry.
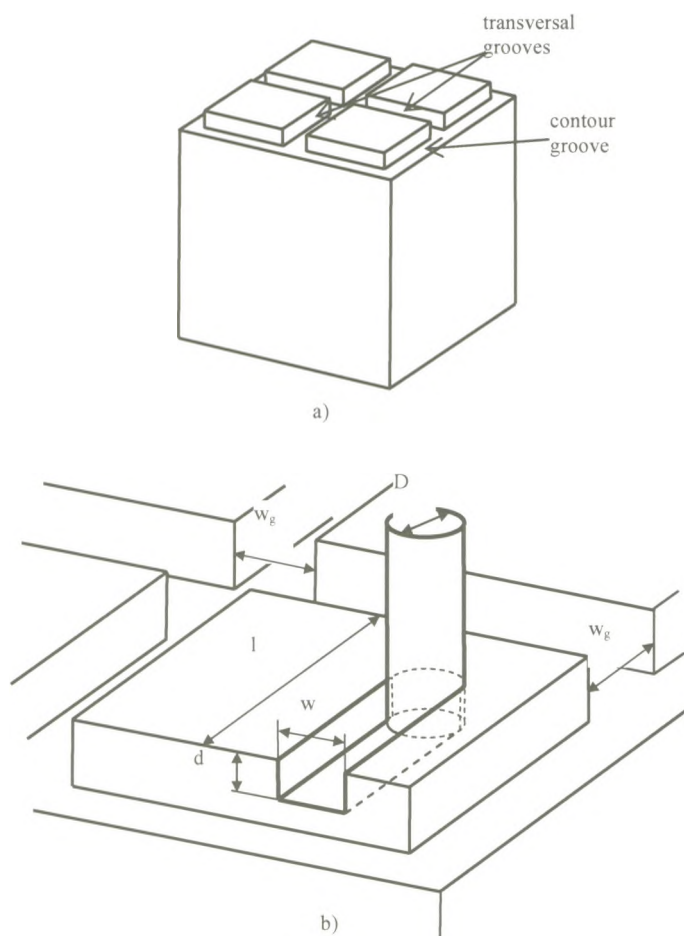
Figure 2-8: Cutting sample: a) preparation of the top surface; and
b) microslot geometry.

2.4.3   Results and Discussion

Examination of the bottom surface of the microslot under scanning electron microscope (SEM) reveals the presence of the porosity closure phenomenon (Figure 2-9). Under the action of the microtool, the continuous material surrounding the pores is pushed towards the adjacent pore whose open area shrinks in size visibly. One of the possible explanations of the phenomenon would be that the microburrs generated at the pore boundaries by the interrupted chip formation are deformed into the surrounding open areas under the pressure exerted by the microtool. Depending on the direction of rotation for the micromill, the microburrs formed on one side of the pore are pushed towards the cavity of the adjacent pore, while those located on the opposing edge – which do not have a neighbouring void to fill – are probably sheared and then removed with the cutting motion of the microtool, since they are not visible. Although the amount of porosity closure represents a major concern for many applications involving porous sintered metals, the irregular contour of the pores and the randomness of their three-dimensional profile make estimation of the reduction in surface area caused by the micromachining process relatively difficult, especially when approached in a strictly deterministic sense.
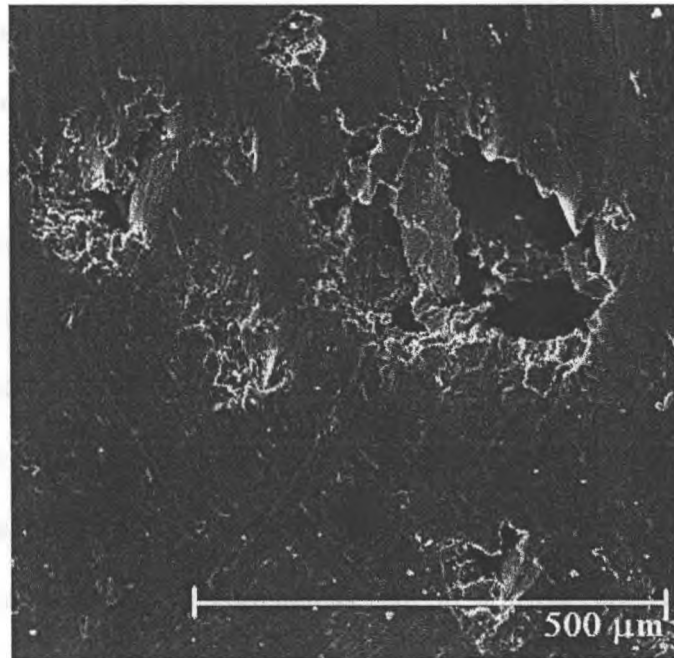
Figure 2-9:   SEM close-up outlining porosity closure mechanism.

The presence of surface smearing phenomenon in micromilling of porous metals could be regarded as an indication of an underlying mechanism based on deformation cutting theory that was originally developed in the context of macroscale machining as detailed in Section 2.1.2. However, the principal critique brought to interrupted cutting theory [28] is no longer valid, since cutting edges and pores are characterized by comparable sizes in micromachining. As a result, a more in-depth investigation of the balance between the two main cutting mechanisms in microscale machining will be required in the future.

Besides porosity closure, the other important parameter that can be used to describe microtool action on the workpiece material is cutting force. A typical three-axial

variation of the cutting force magnitude during microslot cut both in a continuous and a porous titanium sample is depicted in Figure 2-10. Visual analysis of the figure reveals that while micromilling of the continuous material yields relatively constant cutting forces, significant variation in their magnitudes can be noticed while micromachining the porous metal. Moreover, due to the small ratio between tool and pore sizes, the decrease in cutting force magnitude can be correlated well with the porosities encountered along the tool path, especially for Y and Z components of the cutting force. The most notable F_Y and F_Z drop was recorded roughly between 2.5 and 3.3 mm microslot length and it corresponds to the large and deep porosity that is noticeable in a corresponding area of the material. Similar qualitative correlations, but to a lesser degree, can be made concerning some other areas of the microslot.

solid Ti

porous Ti

a) machined slot

b) F_X component of the cutting force

c) F_Y component of the cutting force

d) F_Z component of the cutting force

Figure 2-10: Comparison of cutting forces during slot micromilling of solid and porous

Due to the large tool to pore ratio, correlation between porosity and cutting forces in macroscale domain has been always reduced either to empirical formulations or to extensions of the cutting force models developed for continuous materials (Section 2.2.2). In either case, the cutting force was always measured and reported in an averaged manner and no detailed analysis of the cutting force per revolution has been performed since it is very likely that no major differences would have been noticed anyway between porous and continuous materials. In micromachining, the comparable ratio between tool and pore size makes instantaneous or per revolution analysis of the cutting force an interesting approach since its magnitude variations can be correlated with the amount of porosity encountered along the intended tool path. Accurate porosity estimations performed through image analysis methods in advance of the cut can be used as a cutting force predictor that in turn will provide valuable information on porous metal machinability and implicitly on tool durability. Hence, the correlations between porosity and cutting forces represent one of the most significant performance parameters to be investigated in micromachining operations.

2.5   Conclusions and Future Work

This paper presents a systematic review of the existent literature pertaining macroscale machining of the porous metals. Furthermore, micromilling experiments of porous titanium samples were performed in order to analyze through an original method the impact of the porosity distribution on the magnitude of the cutting forces. The main conclusions of this work can be summarized as follows:

1. None of the two cutting theories proposed for macroscale machining of porous sintered metals is characterized by a good agreement with experimental results, possibly because

of an underestimated effect of the material microstructure. While various alternatives have been suggested to improve their machinability, almost no specific cutting force models have been proposed for these materials. This could be a consequence of the relatively large tool size to pore size ratio that tends to preserve the similarities between these operations and their continuous cutting equivalents.

2. Due to the inherent novelty of the area, no micromachining models were proposed so far for porous metals. Previous works on heterogeneous materials or tungsten copper indicated that small tool to pore size ratio favours large variations in cutting force magnitude. An original method based on visual analysis was devised in this study to determine the correlation between micromilling force and porosity distribution.

3. Similar to macroscale operations, the microslot cutting experiments performed in this work on porous titanium confirmed the presence of the porosity closure phenomenon, along with an evident correlation between cutting force magnitude and size of the pores encountered along the tool path.

4. As hypothesised in macroscale machining, the microstructure plays a significant impact on the dynamics of the material removal operations performed on metallic porous materials. However, while in this case most of the experiments seem to favour the deformation cutting theory, or at least its more pronounced influence on the cutting mechanism, the small tool to pore ratio characteristic to micromachining could determine a transition of the cutting dynamics towards interrupted cutting.

Since the assessment of the porosity closure, as well as of the correspondence between cutting force and pore size that were performed in this study had a strictly qualitative

nature, future work will attempt to characterize it in a quantitative manner. This will provide more insights on the mechanics of cutting as experienced during micromachining of the porous sintered metals in particular and any other type of porous metallic material in general. Development of such theoretical models is expected to enhance the machinability of these materials, prolong the life of the tools and make more accurate predictions regarding machining parameters that are required in order to preserve certain porosity characteristics as dictated by the specific application of the porous sintered metals.

2.6   References

1. Gauthier, M., Lefebvre, L.P., Thomas, Y., and Bureau, M.N., (2004), "Production of metallic foams having open porosity using a powder metallurgy approach," Materials and Manufacturing Processes, 19, pp. 793-811.

2. Lefebvre, L.P, Banhart, J., and Dunand, D.C., (2008), "Porous Metals and Metallic Foams: Current Status and Recent Developments," Advanced Engineering Materials, 10, pp. 775 – 787.

3. Kubicki, B., (1995), "Sintered machine elements," Ellis Horwood, New York.

4. Levina, D.A., Chernyshev, L.I., and Mikhailovskaya, N.V., (2007), "Contemporary powder metallurgy: Achievements and problems," Powder Metallurgy and Metal Ceramics, 46, pp. 202-205.

5. Smith, G.T., (1998), "Getting the measure of PM machinability," Metal Powder Report, 53, pp. 31-35.

6. Cheung, S., Gauthier, M., Lefebvre, L.P., Dunbar, M., and Filiaggi, M., (2007), "Fibroblastic interactions with high-porosity Ti-6Al-4V metal foam," Journal of Biomedical Materials Research Part B: Applied Biomaterials, 82, pp. 440-449.

7. St-Pierre, J.P., Gauthier, M., Lefebvre, L.P., and Tabrizian, M., (2005), "Three-dimensional growth of differentiating MC3T3-E1 pre-osteoblasts on porous titanium scaffolds," Biomaterials, 26, pp. 7319-7328.

8. Baril, E., Lefebvre, L.P., Thomas, Y., and Ilinca, F., (2008), "Foam-coated MIM gives new edge to titanium implants," Metal Powder Report, 63, pp. 46-50.

9. Hallab, N.J., Jacobs, J.J., and Katz, J.L., (2004), "Orthopedic applications", in Biomaterials Science, An Introduction to Materials in Medicine, Elsevier Academic Press, San Diego, CA, pp. 526-555.

10. Kalorama Information, 2009, "Implant-Based Dental Reconstruction: World Dental Implant and Bone Graft Market, 3rd Edition."

11. Neumann, P., (1999), "Porous metal structures made by sintering: processes and applications," in Proceedings of the 1st International Conference on Metal Foams and Porous Metal Structures (MetFoam'99), June 1999, Bremen, Germany, pp. 167-170.

12. Banhart, J., (2001), "Manufacture, characterisation and application of cellular metals and metal foams," Progress in Materials Science, 46, pp. 559-U3.

13. Mott Corporation, (1996), "Porous Metal Products for OEM Applications," In Mott Technical Handbook, Sections 1000-9000.

14. Eisenmann, M., (1998), "Porous Powder Metallurgy Technology," in ASM Handbook,7: Powder metal technologies and applications, ASM International, Materials Park, OH, pp. 1031-1042.

15. Chopra K.S., (1988), "Manganese sulfide in machining grade ferrous P/M alloys," in: Modern Developments in Powder Metallurgy, 21, edited by , P.U. Gummeson and D.A. Gustafson, Metals Powder Industries Federation, Princeton, NJ, pp. 361–379.

16. Lefebvre L.P., and Thomas, Y., (2003), "Method of making open cell material," United States Patent No. 6660224.

17. Cominotti, R. and Gentili, E., (2008), "Near net shape technology: An innovative opportunity for the automotive industry," Robotics and Computer-Integrated Manufacturing, 24, pp. 722-727.

18. Holzki, M., (1996), "Optimization of Cutting Parameters when Drilling Sintered Stainless Steel 430LHC," Powder Metallurgy, 39, pp. 256-258.

19. Alizadeh, E., (2008), "Factors influencing the machinability of sintered steels," Powder Metallurgy and Metal Ceramics, 47, pp. 304-315.

20. Geijer, E., and Jamison, R.B., (1979), "Machinability of Sintered Iron," in: Source Book on Powder Metallurgy, edited by S. Bradbury, American Society for Metals: Metals Park, OH. pp. 256-278.

21. Chadwick, G.A., and Kehoe, F.P., (1995), "Machinability of Sintered Ferrous Powder Metallurgy Compacts," in: Report Chandlers Ford, Eastleigh.

22. Causton, R.J., (1995), "Machinability of the P/M Steels," in: Proceedings of the International Conference on Powder Metallurgy and Particulate Materials, May 1995, Seattle, WA, last retrieved from: http://www.hoeganaes.com/navpages/NewTechbyTopic/TechbyTopicv2/TechPapersv2/35.pdf

23. Toenshoff, H.K., Wobker, H.-G., Fritsch, A., (1995), "Machining of Powder Metallurgy Materials," in: Advances in Powder Metallurgy and Particulate Materials, 8, Compiled by Philips M., and Porter , J., Metals Powder Industries Federation, Princeton, NJ, pp. 105-128.

24. Engstrom, U., (1983), "Machinability of Sintered Steels," Powder Metallurgy, 26, pp. 137-144.

25. Shareef, I. and Boswell, K.H., (1994), "Production Models for Drilling Sintered Steel," in: Advances in Powder Metallurgy and Particulate Materials, 7, Compiled by Lall, C., and Newpaver, A.J., Metals Powder Industries Federation, Princeton, NJ, pp. 153-

26. Causton, R.J., and Cimino, T., (1998), "Machinability of P/M steels," in: ASM Handbook, 7: Powder Metal Technologies and Applications, ASM International, Materials Park, OH, pp. 671–680.

27. Chandler, E., (1990), "Machining of Powder Metallurgy Materials," in: ASM Handbook, 16: Machining, ASM International, Materials Park, OH, pp. 879-892.

28. Agapiou, J.S. and Devries, M.F., (1988), "Machinability of Powder-Metallurgy Materials," International Journal of Powder Metallurgy, 24, pp. 47-57.

29. Salak, A., Selecka, M, and Danninger, H., (2005), "Machinability of Powder Metallurgy Steels," Cambridge International Science Publishing, Cambridge, U.K.

30. Danilenko, V.A., (1968), "Study of the surface layers of machined porous materials by the eddy current method," Powder Metallurgy and Metal Ceramics, 7, pp. 105-106.

31. Roy, L.G., de Rege, A.F., and Pease, L.F., (1988), "Relationship between machinability and strength in a prealloyed manganese sulphide sintered material," in: Powder Metallurgy. World Congress and Exhibition, 21, Metal Powder Industries Federation, Princeton, NJ, pp. 327–360.

32. Young, B.A., (2002), "Optimization of PCBN Cutting Tools for Machining of Ferrous P/M Parts", in: Proceedings of International Conference on Powder Metallurgy & Particulate Materials (PM2TEC), New Orleans, FL.

33. Chagnon, F. and Gagne, M., (1998), "Machinability Characterization of P/M Materials," Transactions of SAE, 107, pp. 416-420.

34. Bernhardt, C., Husemann, K., and Heegn, H., (1977), "Effect of milling conditions on the densification of metal powders in pressing and sintering," Powder Metallurgy and Metal Ceramics, 16, pp. 238-42.

35. Bram, M., Kempmann, C., Laptev, A., Stover, D., and Weinert, K., (2003), "Investigations on the machining of sintered titanium foams utilizing face milling and peripheral grinding," Advanced Engineering Materials, 5, pp. 441-447.

36. Bram, M., Laptev, A., Buchkremer, H.P., and Stover, D., (2005), "Application of powder metallurgy for the production of highly porous functional parts with open porosity," Materials Forum, 29, pp. 119-122.

37. Zurecki, Z., Ghosh, R., and Frey, J.H., (2004), "Finish-turning of hardened powder metallurgy steel using cryogenic cooling," International Journal of Powder Metallurgy, 40, pp. 19-31.

38. Ives, R.L., Falce, L.R., Schwartzkopf, S., and Witherspoon, R., (2005), "Controlled porosity cathodes from sintered tungsten wires," Ieee Transactions on Electron Devices, 52, pp. 2800-2805.

39. Tarter, J.O., Effgen, M., Pusavec, F., and Jawahir, I.S., (2008), "Cryogenic machining of porous tungsten for dispenser cathode applications," in: Vacuum Electronics Conference, (IVEC2008), IEEE International, New York, pp. 291-292.

40. Deglurkar, M., Davy, D.T., Stewart, M., Goldberg, V.M., and Welter, J.F., (2007), "Evaluation of machining methods for Trabecular Metal implants in a rabbit intramedullary osseointegration model," Journal of Biomedical Materials Research Part B-Applied Biomaterials, 80B, pp. 528-540.

41. Metal Powder Industries Federation, "Porous Metal Design Guidebook," last retrieved from: www.mpif.org/DesignCenter/porous.pdf

42. Trent, E.M., (1977), "Metal Cutting," Butterworths, London, UK.

43. Claeys, S.F. and Chopra, K.S., (1998), "Enhanced machinability and oxidation resistance of P/M steels using modified MnS additions," International Journal of Powder Metallurgy, 34, pp. 29-36.

44. Robert-Perron, T. and Blais, C., (2008), "Green machining: Parameters, applications, and sintered properties," International Journal of Powder Metallurgy, 44, pp. 41-48.

45. Madan, D.S., (1995), "Importance of Machinability in the Processing of P/M Parts," in: Advances in Powder Metallurgy and Particulate Materials, 2, Compiled by Philips M., and Porter , J., Metals Powder Industries Federation, Princeton, NJ, pp. 8/55-8/68.

46. Chen, S., Head, D., Effgen, M., and Jawahir, I.S., (2005), "An investigation of sustained machining performance for controlled surface quality requirements in porous tungsten," IEEE Transactions on Electron Devices, 52, pp. 903-908.

47. Salak, A., Selecka, M., and Bures, R., (2001), "Manganese in Ferrous Powder Metallurgy," Journal of Science and Technology of Particle Materials, 1, pp. 41-58.

48. Robert-Perron, E., Blais, C., Thomas, Y., Pelletier, S., and Dionne, M., (2005), "An integrated approach to the characterization of powder metallurgy components performance during green machining," Materials Science and Engineering A: Structural Materials Properties Microstructure and Processing, 402, pp. 325-334.

49. Agapiou, J.S., Halldin, G.W., and Devries, M.F., (1989), "Effect of Porosity on the Machinability of P/M-3041 Stainless-Steel," International Journal of Powder Metallurgy, 25, pp. 127-139.

50. Armarego, E.J.A., Shi, G., and Verezub, S., (2001), "Modelling the basic cutting action and machining performance of sintered metallic materials," Machining Science and Technology, 5, pp. 353-373.

51. Artamonov, A.Y. and Kononenko, V.I., (1967), "Cutting forces in machining porous cermets," Powder Metallurgy and Metal Ceramics, 6, pp. 584-588.

52. Kas'yan, M.V. and Zaimtsyan, G.M., (1973), "Effect of porosity on cutting forces," Powder Metallurgy and Metal Ceramics, 12, pp. 481-484.

53. Kryukovskii, V.V., Ognev, R.K., and Zaikin, Y.K., (1980), "Machinability of sintered titanium," Powder Metallurgy and Metal Ceramics, 19, pp. 471-473.

54. Dornfeld, D., Min, S., and Takeuchi, Y., (2006), "Recent Advances in Mechanical Micromachining," CIRP Annals - Manufacturing Technology, 55, pp. 745-768.

55. Masuzawa, T., (2000), "State of the art of micromachining," CIRP Annals 2000: Manufacturing Technology, 49, pp. 473-488.

56. Liu, X., DeVor, R.E., Kapoor, S.G., and Ehmann, K.F., (2004), "The mechanics of machining at the microscale: Assessment of the current state of the science," Journal of Manufacturing Science and Engineering: Transactions of the ASME, 126, pp. 666-678.

57. Chae, J., Park, S.S., and Freiheit, T., (2006), "Investigation of micro-cutting operations," International Journal of Machine Tools & Manufacture, 46, pp. 313-332.

58. Uhlmann, E., Piltz, S., and Schauer, K., (2005), "Micro milling of sintered tungsten-copper composite materials," Journal of Materials Processing Technology, 167, pp. 402-407.

59. Vogler, M.P., DeVor, R.E., and Kapoor, S.G., (2003), "Microstructure-level force prediction model for micro-milling of multi-phase materials," Journal of Manufacturing Science and Engineering: Transactions of the ASME, 125, pp. 202-209.

60. Vogler, M.P., DeVor, R.E., and Kapoor, S.G., (2004), "On the modeling and analysis of machining performance in micro-endmilling, Part I: Surface generation," Journal of Manufacturing Science and Engineering-Transactions of the ASME, 126, pp. 685-694.

61. Vogler, M.P., Kapoor, S.G., and DeVor, R.E., (2004), "On the modeling and analysis of machining performance in micro-endmilling, Part II: Cutting force prediction," Journal of Manufacturing Science and Engineering: Transactions of the ASME, 126, pp. 695-705.

Chapter 3

3 Optical-Based Image Analysis of Porosity in Micromilling of Titanium Foams

3.1 Introduction

Porous sintered metals are typically produced by powder metallurgy and represent a class of relatively new materials with wide variety of industrial applications, especially biomedical applications, e.g. dental and orthopaedic applications [1-3], due to their light weight, high strength, and full biocompatibility properties. However, outer surface geometry and porosity topology for fabricated components, e.g. implants and prostheses, significantly influence the adherence of bone cells to implant material. Therefore, most components fabricated from porous foam metals are produced in near-net shapes, and still require secondary machining operations [4] that can provide the desired roundness, smearing and other surface quality parameters which cannot be obtained during sintering [5]. Also, there are many 3D shapes and geometries that are difficult or almost impossible to produce by conventional forming technologies [2] without secondary machining, e.g. slots, bevels, blind holes, threads, cross-holes and re-entrants normal to the pressing directions. At present, about half of the components produced by powder metallurgy parts require secondary machining operations [6]. New microfabrication technologies, such as micromilling and laser micromachining [7], opened new technological possibilities in porous material geometry modification by allowing a superior control of surface roughness and even porosity closure amount. These two surface characteristics influence to a large extent the friction coefficient between implant and surrounding bone tissue. However, two main interrelated technical challenges are associated with obtaining of the

desired surface geometry and roughness on outer porous surfaces: accurate characterization of real 2D/3D porosity values and optimization of micromachining process parameters with respect to the physical porosity amounts. From this perspective, the present study focuses on optical image analysis of porosity with respect to material removal process through micromilling operations.

Physical-mechanical properties of porous metals and their adherence with bone cells significantly depend on 2D/3D porosity characterized through parameters like: quantity of pores (i.e., the fractional porosity), interconnectivity, size, morphology, permeability, and spatial distribution [8-11]. Classical non-destructive optical image analysis methodologies have been successfully applied in the past to analysis of cell morphology and microstructure of porous metals [8]. In most cases, pore size distribution and shape analysis was performed by means of commercial image analysis programs. The main drawback of this approach resides in destructive techniques involved in preparation of sample surface because image analysis is significantly dependent on appropriate differentiation between solid material and internal cavities. Optical image analysis is limited to 2D spatial analysis only. Nevertheless, optical micrographs were used before in the context of porous Ti materials used in load-bearing implants [12]. Within machining environment, the most common application of vision-based methods is represented by tool wear analysis and monitoring [13-17]

New developments in X-ray based micro computer tomography (micro-CT) have opened advanced non-destructive options for characterization and visualization of 3D foam structures [11]. The micro-CT technique performs segmentation of 3D porosity into a set of 2D CT slice images providing acceptable image quality, precise density profile, high

spatial resolutions (i.e. below 1 μm), good pore contrast, and reliable pore shape anisotropy. Micro-CT is still under development especially in terms of 3D structure reconstruction and extraction of reliable information on structural parameters [18,19].

As mentioned above, metal foam based functional components (e.g. biomedical implants and prostheses) require a rough outer surface with fully open pores in order to attain high levels of bonding between implant and bone. Among the options available to generate implant surfaces, material removal operations have always been well regarded, especially when moving into the micro-scale domain. In this sense, the use of small diameter cutting tools (around 25 μm) in micromilling operations is believed to be capable of significantly enhancing the accuracy of the generated surfaces. However, when the size of the cutting tools becomes comparable with pore size, this induces significant fluctuations in the cutting force [20] leading to excessive tool wear and/or breakage. Cross-correlation between micromachining parameters and porosity has been relatively little investigated in the literature and therefore represents one of the objectives of the current work.

Intuitively, it is easy to understand that each micromilled slot cut in a porous sample will be characterized by a unique process signature that is strongly dependent on porosity distribution. This difference was outlined in the past [20] by comparing resultant cutting forces during micromilling of solid and foam Ti. As shown in Figure 3-1, the resultant cutting force amplitude is increased (0.52N vs. 1.05N) and peak-to-valley magnitude of the cutting force is reduced (0.4N vs. 0.1N) when micromilling porous compared to solid titanium.
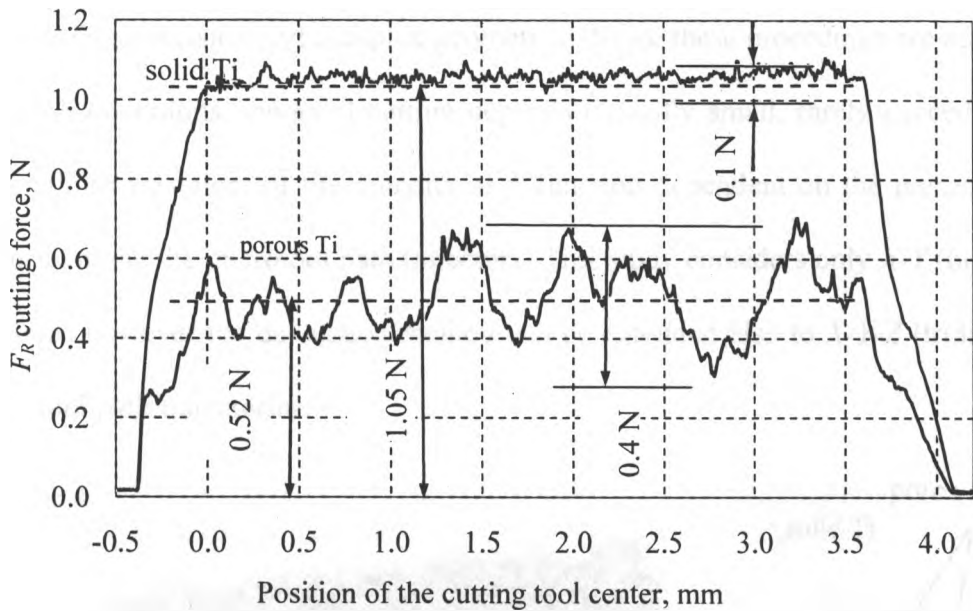
Figure 3-1: **Comparison of resultant cutting forces measured during micromilling of solid and porous Ti [20]**

The present research is primarily focused on the development of an optical image processing method for analysis of surface porosity with respect to the in-rotation microcutting edge trajectory. For this purpose, optical images of the micromachined surface are acquired and then the proposed method is used to determine the fraction of solid material removed during each tool revolution. Finally, the cross-correlation between surface porosity and resultant cutting force will be estimated.

3.2 Vision-Based Estimation of Porosity during Micromilling Operations

Functional parts and components made from Ti-6Al-4V foams are characterized by a complex 3D porosity with significant variations in pore size and morphology as shown in Figure 3-2. For these materials, micromilling with cutting tools having a diameter smaller

than 0.4 mm can be used as a secondary shaping procedure that is capable of achieving high surface precision and complex geometries. Since these procedures are accounted for as finish operations, the axial cutting depth is typically small, rarely exceeding 20 μm. This allows treatment of the porosity as a function dependent on the presence of solid material along the microtool path trajectory. This study considers only X-Y (planar/linear) motions, however the developed method can be extended also to X-Y-Z (tridimensional) microtool path trajectories.
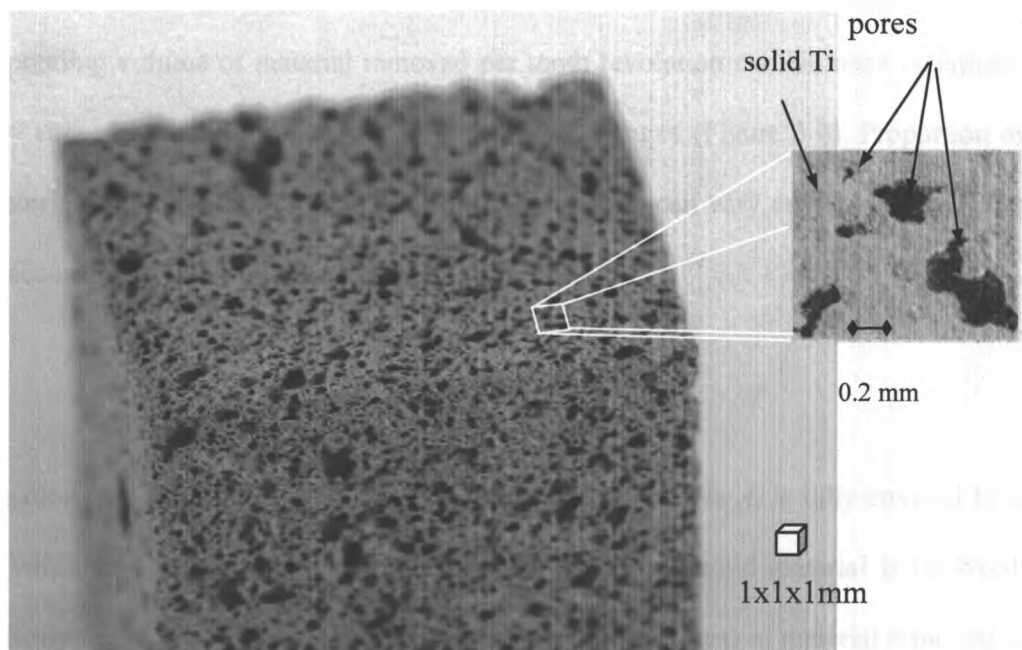
Figure 3-2: **Typical sample of a porous Ti foam (Ti-6Al-4V) characterized by a complex 3D porosity structure**

During microslot end-micromilling, each cutting tooth moves along the trochoidal trajectory formed as a superposition of tooth rotational motion around the cutter axis and linear translation of tool center along the intended tool path, as shown in Figure 3-3. In this case, the area swept per i-th tool revolution A_i, represents the geometric difference between two consecutive, i-th and $(i-1)$-th, cutting tooth trajectories. This area can be

approximated as the difference of two consecutive circles separated by a feed per tooth value, f (Figure 3-3). When machining solid material, the area S_i and the volume of material removed per tooth revolution V_i, will be always constant: S_i, V_i = const. Moreover, the swept area A_i, and area of material removed, S_i per tooth revolution are absolutely identical.

By contrast, the presence of randomly distributed porosity makes the estimation of the amount of solid material removed more difficult. In this situation, the area and the corresponding volume of material removed per tooth revolution exhibit large variations, S_i, V_i = var., although the swept area A_i, remains unchanged (Figure 3-4). Proportion of the material within the swept area per tooth revolution p_i can vary anywhere between 0 and 1 according to the following relationship:

$$p_i = \frac{S_i}{A_i} \qquad (1)$$

In Equation (1), $p_i = 0$ corresponds to the case when swept area A_i is fully covered by a pore (void), and $p_i = 1$ corresponds to the case when only solid material is removed. Because cutting force is directly proportional to the volume (area) of material removed, it is important to recognize that cutting forces will vary with respect to porosity, specifically the fraction of solid material contained within the area removed during one complete revolution of the cutter. This fraction will be quantified herein based on optical considerations.
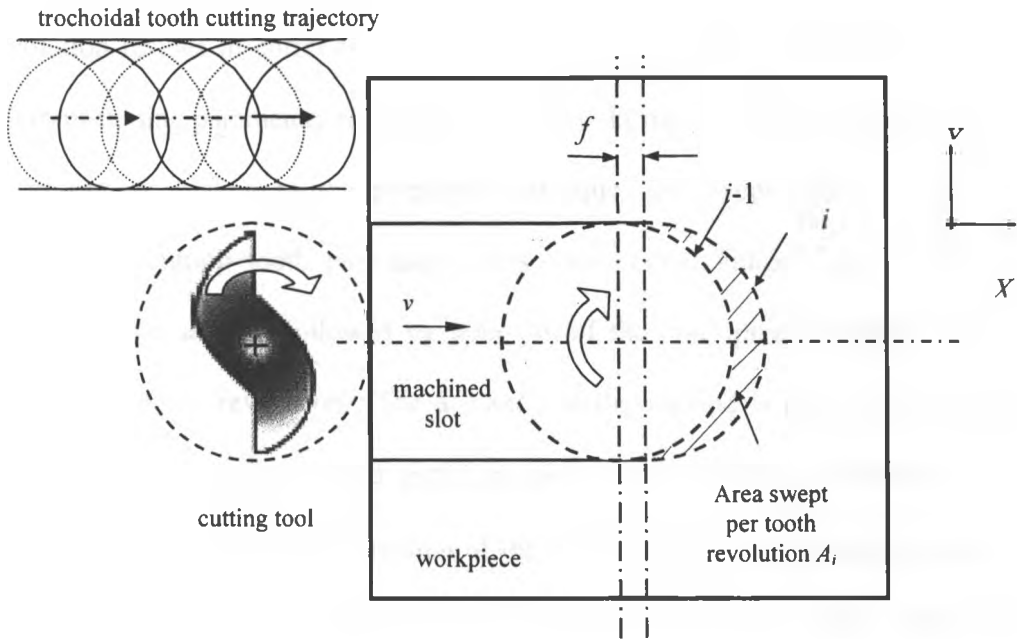
Figure 3-3: Area removed during one tooth revolution
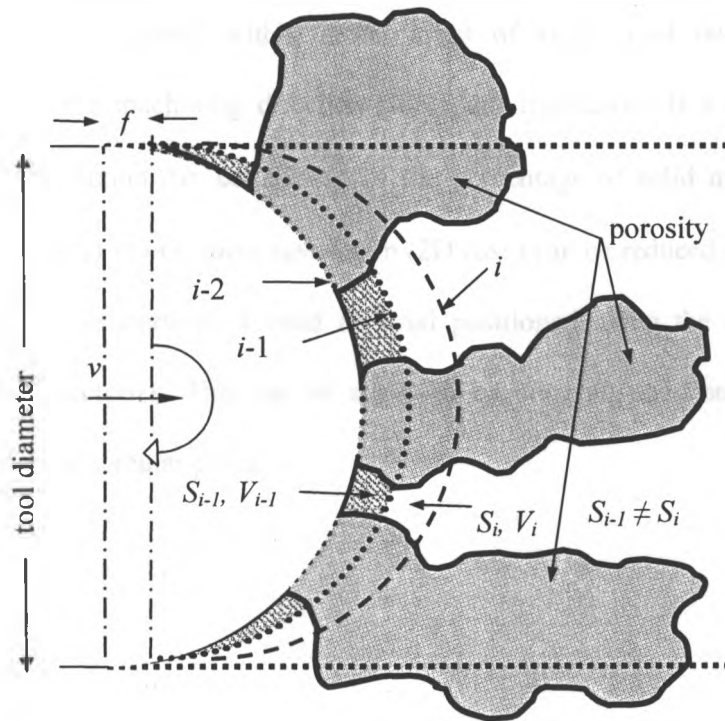
Figure 3-4: Visual appearance of porosity enclosed within the area swept in one cutter revolution

The novelty of the methodology proposed for estimation of the porosity fraction per tool revolution resides in correlation of the optical images of the micromilled surface with micromachining parameters recorded in real-time during cutting (cutting forces and axial positions). According to the proposed technique, the swept area is determined by overlapping cutting tooth path trajectories with optical images acquired for the top surface of the sample, followed by selection of the "on" pixels located between two consecutive tooth revolutions. The accuracy of the method is primarily influenced by optical image resolution Δh, and spatial sampling period of linear tool motions Δl. Figure 3-5 depicts a graphical representation of the area covered in one tooth revolution. Each tooth path is offset with a distance equal to feed per tooth f. After swept area and corresponding pixels for each tooth revolution are determined, the porosity and the material presence contained within swept areas of single tool revolutions can be calculated along the machining direction (tool path trajectory). If f is comparable to optical image resolution Δh, calculation of the percentage of solid material contained within the area swept in one cutter revolution (2D case) can be reduced to an 1D problem by estimating the proportion of solid material positioned along the circumference of circular tooth trajectories. This can be achieved by counting the "on" pixels that are intersected by these circular paths.
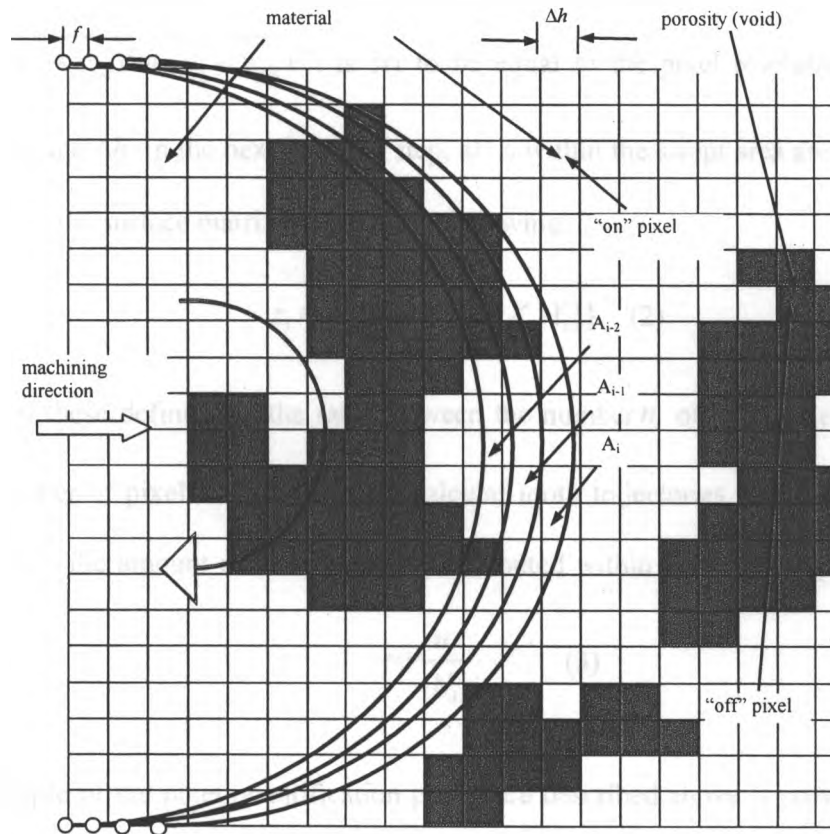
Figure 3-5: **Estimation of material presence within the area swept in one cutter revolution**

The optical image has to be initially pre-processed to a binary format such that it contains only white ("on") and black ("off") pixels that correspond to solid material and pores, respectively. As a result, the surface is converted to an array $[X_i, Y_i, Z_i]$ defined only through zeros ($Z_i = 0$ for solid material) and ones ($Z_i = 1$ for voids). After that, tooth trajectories are calculated based on the position in real time of the bottom tool center and tool size. The newly obtained tooth trajectories are then overlapped with the optical image, such that each tooth trajectory becomes a vector with $\{x_i, y_i, z_i\}$ components. The z_i values are initially unknown as they correspond to material presence for a particular (x_i,

y_i) location. It is also necessary to note that the sampling period of the tooth trajectory,

$\Delta l = \sqrt{(x_j - x_{j-1})^2 + (y_j - y_{j-1})^2}$, is set to be equal to the pixel resolution of acquired

optical image Δh. In the next iteration step, all z_i within the swept area are determined as

a subset of the surface matrix $[X_i, Y_i, Z_i]$ as following:

$$z_i = \{Z_i \mid \{x_i, y_i\} \cap [X_i, Y_i]\} \quad (2)$$

Based on these definitions, the ratio between the number n_i of "on" pixels ($z_i = 0$) and

total number of pixels intersected by particular tooth trajectories N_i will be fractionally

identical to the amount of solid material distributed within the area swept in one cutter

rotation:

$$p_i = \frac{n_i}{N_i} \qquad (3)$$

An example of the pixel quantification procedure described above is provided in Figure

3-6
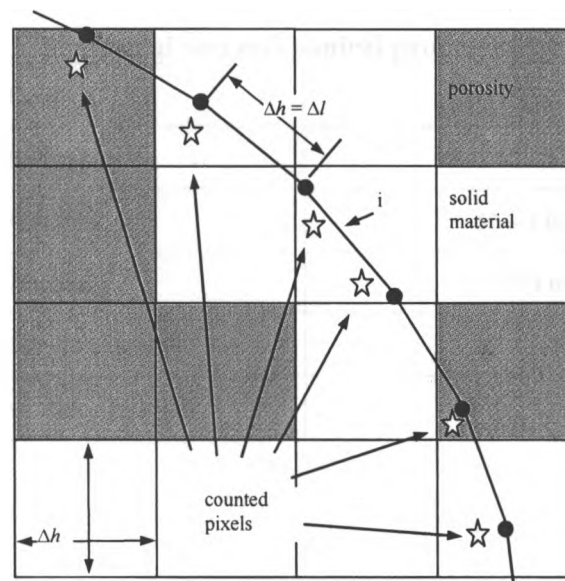
Figure 3-6: **Accounting for pixels and their associated material/void attributes along circular tooth paths**

3.3   Experimental Verification

Applicability of the developed approach for vision-based estimation of porosity was verified experimentally in the context of porous Ti foam micromilling. Real-time measurements of cutting forces and motions were performed during cutting trials. Then, the actual porosity per single tooth revolution was estimated and subsequently correlated to instantaneous cutting force magnitudes.

3.3.1   Material Description

The Ti-6Al-4V foam used in micromilling trials was manufactured by Industrial Material Institute of the National Research Council of Canada (Boucherville, Quebec) by means of a patented powder metallurgy procedure [21]. Structural and mechanical properties of the Ti foam are presented in Table 1. The samples had a cubic shape with an approximate side length of 13 mm (Figure 3-2). Multiple samples were cut in order to stabilize the experiments.

Table 3-1:   Structural and mechanical properties of Ti foam [3]

Density	$1.6 - 2.25$ g/cm^3
Porosity	$50 - 65$ %
Pore size	$50 - 1400$ µm
Surface area	0.05 m^2/g
Compressive yield strength	$25 - 125$ MPa
Compressive elastic modulus	$5 - 20$ GPa

3.3.2   Experimental Setup and Methodology for Micromilling

Micromilling experiments were carried out on a custom-built five-axis CNC micromilling system equipped with an air-bearing spindle capable of rotational speeds between 5,000 and 100,000 rot/min range. The system is capable of providing a static positional accuracy of 1 μm over a 300 mm maximum travel range.

Cutting experiments were performed as micromilling of linear slots along X-axes using a two-flute, uncoated, tungsten carbide flat end micromill having a diameter of 800 μm diameter and helix and clearance angles of 25° and 6°, respectively. Linear slots having a width of 800 μm, depth of 40 μm and length of 12 mm were machined on the top face of the foam Ti specimen with a feed rate of 120 mm/min and spindle rotational speed of 10020 rot./min.

An in-house developed real-time data acquisition system written in Labview was used to measure the X, Y, and Z components of the cutting force with a Kistler dynamometer (type 9256C2) and a Kistler dual mode charge amplifier (type 5010B). The X, Y, and Z cutting motions were tracked based on a signal from position encoders and three-phase current consumed by spindle drive. Spindle current and cutting forces $F(t) = \{F_X(t), F_Y(t), F_Z(t)\}$, were recorded with a sampling frequency of 25 kHz with a minimum threshold of 0.002 N and were filtered out of the resonance frequency of the dynamometer (around 4.8 kHz). Simultaneously, the cutting position $l(t) = \{l_X(t), l_Y(t), l_Z(t)\}$, along the tool path trajectory was recorded with a sampling frequency of 500 Hz. Further, a mean value of the cutting force in each direction was calculated for each tooth revolution using spindle current signal as point of synchronization in space domain. After that, cutting forces were

rearranged as a spatial function of the cutting tool path trajectory $F(l) = \{F_X(l_X), F_Y(l_Y),$ $F_Z(l_Z)\}$, using synchronization in time domain between cutting forces and their corresponding axial positions.

3.3.3 Experimental Setup and Methodology for Image Analysis of Porosity

Optical image acquisition of micrographs was performed after micromachining by using a CANON EPS 450D camera with a 12.2 megapixel image sensor equipped with an EF 100 mm macro lens (f/2.8 Macro USM) that provides a spatial image resolution Δh of approximately 6 µm/pixel. A custom indirect LED light was used to reduce light reflections and enhance picture contrast for better porosity assessments. In this study, the length of the machined slot was 12.56 mm and the feed per tooth f was 0.012 mm. Due to the comparable values of Δh and f, estimations of the solid material fraction located along the circular tooth trajectory can be performed accurately through the proposed 1D approach as described in Section II, above. It will be assumed here that the porosity has a minimal cross sectional variation over the investigated axial depth of cut (20 – 40 µm) that is characteristic to finish operations. As a result, the porosity amount measured on top of the sample surface before and after the microslot cutting operation will be assumed to be approximately identical.

The general methodology for vision-based estimation of porosity involves the following steps:

(a)   Acquire and convert the optical image of the micromilled surface to the binary format

(b)   Synchronize tooth position with time and superimpose its trajectory on the optical image of the surface

(c)   Perform circular to linear tooth path conversions (e.g. "linearizations")

(d)   Calculate the total number of optical pixels intersected by a singular tooth path N_i

(e)   Calculate the total number of "on" pixels n_i ($z_i = 0$) along the investigated tooth path

(f)   Establish the instantaneous solid material fraction p_i removed during each revolution of the tool (Equation 3)

(g)   Track the instantaneous amount of solid material removed with respect of axial position of the tool $p(l)$

In Step (a), grey-scale micrographs of the sample surface captured by a high resolution camera are converted to binary format by using an appropriate imaging threshold to clearly delimit the porosity (black) and solid material (white). The threshold is set in such way to ensure accurate conversions of voids into black, especially when considering pore boundaries by using Otsu 's method implemented in Matlab (Figure 3-7). Any dark spot covering less than 10 pixels was considered noise (light reflected on non-planar foam inclusions) and therefore was filtered out.
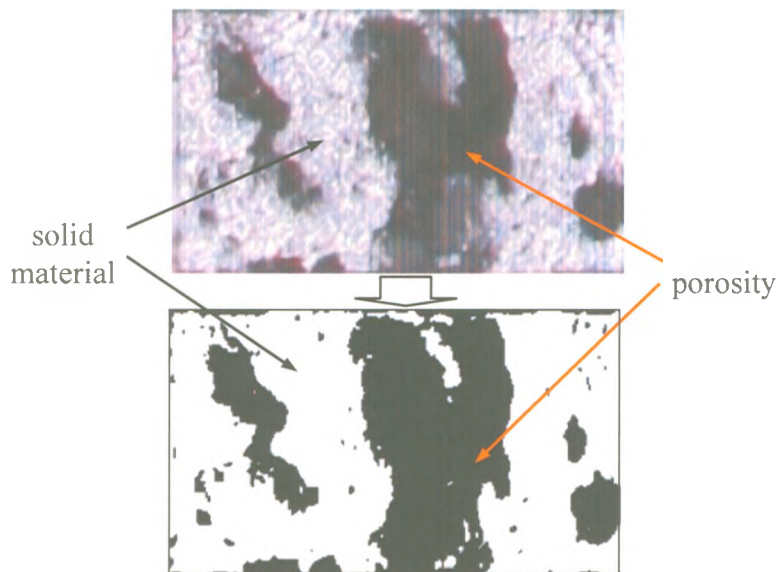
Figure 3-7: **Converting grey porosity micrographs (top) into binary format (bottom) through thresholding**

Figure 3-8 illustrates the Steps (b) to (f) involved in vision-based estimation of the porosity. First, circular trajectories of the cutting tooth rotation along tool path motion are superimposed on the black and white micrographs according to Step (b). Then, in Step (c), the circular tooth trajectory is "linearized". After performing the quantitative assessments involved in Steps (d) through (f), the outcome of Step (g) is a function $p(l)$ expressing the fraction of solid material removed for any instantaneous position of the tool along the intended tool path.
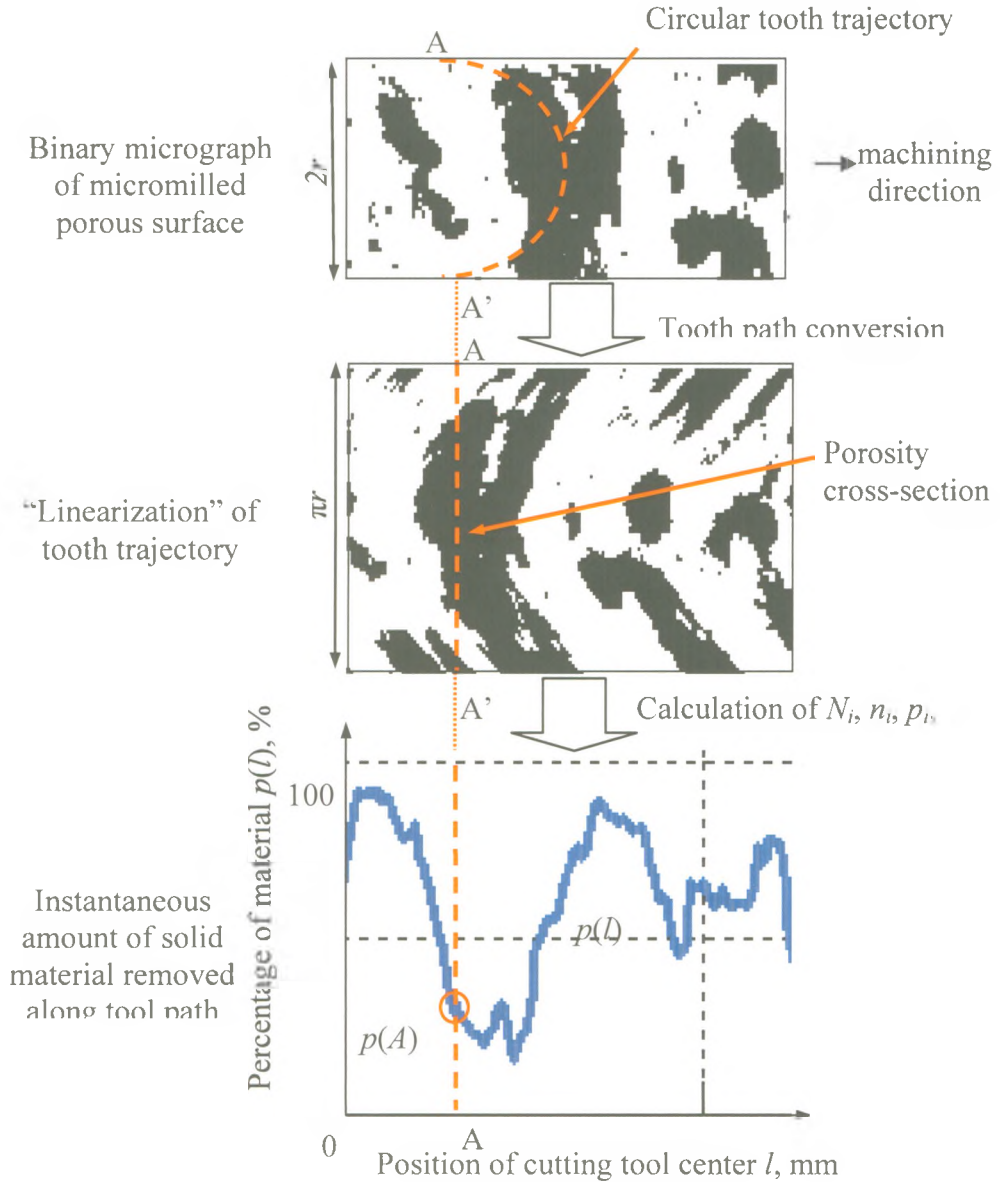
Figure 3-8: **Optical image processing and porosity assessment**

3.3.4 Preliminary Experimental Analysis of Correlation Between Porosity and Cutting Forces

To analyze the interplay between porosity and cutting forces from a statistical standpoint, they should be both dependent on the same variable. For this application, the most

rational choice for the common variable would be the space domain, specifically the instantaneous position of the micromill along its trajectory $l(t) = \{l_X(t), l_Y(t), l_Z(t)\}$. As a result, both porosity and cutting forces were expressed as a function of l, respectively. Figure 3-9 depicts a representative comparison between instantaneous amount of solid material removed and corresponding magnitudes of the resultant cutting force. A simple visual inspection of the graph reveals that cutting force variations follow closely the percentage of solid material removed in each tool revolution.
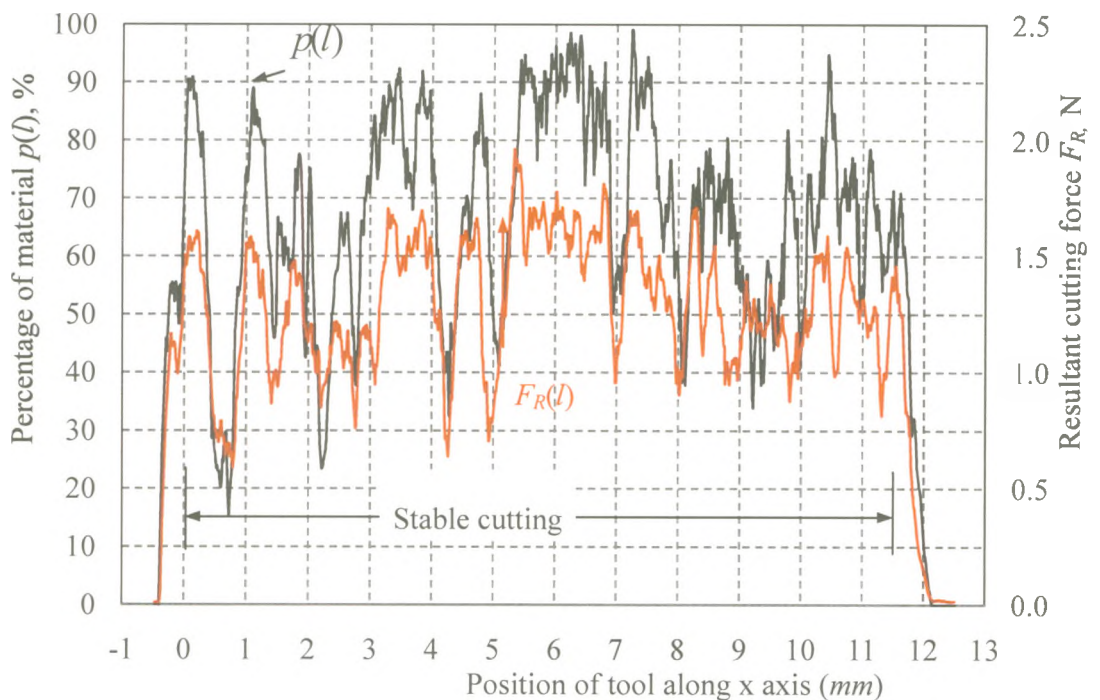
Figure 3-9: **Comparison between instantaneous amount of material removed and resultant cutting force**

Cross-correlation between the instantaneous fraction of material removed in one cutter revolution $p(l)$ and resultant cutting force $F_R(l) = \sqrt{F_x^2(l) + F_Y^2(l)}$, was analyzed further

by means of traditional statistical characteristics, such as correlation coefficient and coherence function [22]. It was found that resultant cutting force is dependent on solid material fraction with a correlation coefficient of 75% during stable micromilling that excludes entering and exiting cutting stages. Coherence function between $p(l)$ and $F_R(l)$ displayed in Figure 3-10 reveals that a significant correlation exists between them in low frequency area, e.g. below 1.6 mm^{-1}.
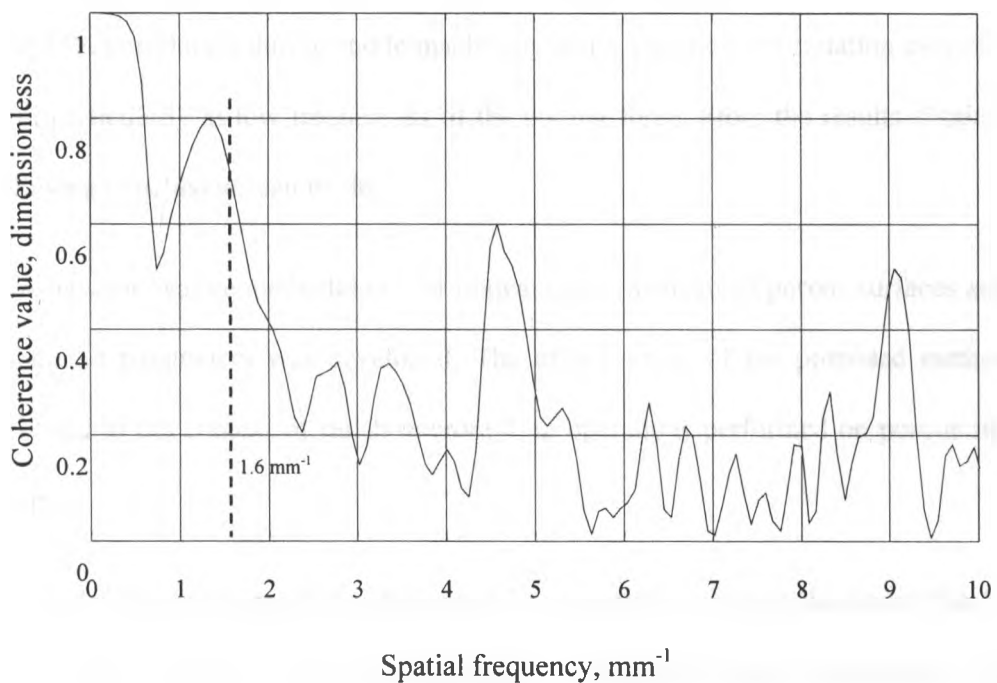
Figure 3-10: Coherence function between proportion of material and resultant cutting force

3.4 Summary and Conclusions

This study proposes an original image analysis approach for optical determination of porosity in context of micromilling operation. The developed technique extracts from an optical image (micrograph) the area of material removed through micromilling and then calculates the fraction of solid material removed in each tool revolution. The proposed methodology was experimentally tested by micromilling a linear slot in porous Ti foam (Ti-6Al-4V). The resultant cutting force is dependent on the proportion of solid material with 75% correlation during stable machining and a significant correlation exist between them particularly at low frequencies of the cutting force. From the results obtained, the following conclusions can be drawn:

1. A new innovative methodology for optical image analysis of porous surfaces and their associated parameters was developed. The effectiveness of the proposed method was validated in the context of finish micromilling operations performed on porous titanium samples.

2. The developed approach involves pixel level quantifications to determine the fraction of solid material removed during each cutter revolution. However, pixel counts might not be accurate enough at low optical image resolutions. More accurate estimation of the area swept per tooth revolution can be achieved by applying an alternative approach where the partial area of each pixel intersected by a tooth trajectory will have to be estimated.

3. It was proved experimentally that the resultant cutting force is dependent on the proportion of material with a correlation coefficient of 75% during stable machining. This correlation is valid only for low-frequency cutting force variations. In the high-

frequency domain, it is expected that the dynamics of the cutting process exerts a predominant influence on variation of the cutting forces.

4. The proposed approach opens up new opportunities in analysis, monitoring, optimization and control of the cutting process during finish micromilling of porous foams aiming generation of optimized microstructural surface geometries in terms of both surface roughness and porosity closures.

3.5 References

1. Banhart J, Weaire D (2002) On the road again: Metal foams find favor. Physics Today 55 (7):37-42.

2. Ryan G, Pandit A, Apatsidis DP (2006) Fabrication methods of porous metals for use in orthopaedic applications. Biomaterials 27 (13):2651-2670.

3. Baril E, Lefebvre L-P, Thomas Y, Ilinca F (2008) Foam-coated mim gives new edge to titanium implants. Metal Powder Report 63 (8):46-50.

4. Smith GT (1998) Getting the measure of pm machinability. Metal Powder Report 53 (5):31-35.

5. Eisenmann M (2000) Porous P/M Technology, ASM Handbook, vol. 7.

6. Alizadeh E (2008) Factors influencing the machinability of sintered steels. Powder Metallurgy and Metal Ceramics 47 (5-6):304-315.

7. Bordatchev E, Nikumb S (2008) Fabrication of moulds and dies using precision laser micromachining and micromilling technologies. Journal of Laser Micro Nanoengineering 3 (3):175-181.

8. Banhart J (2001) Manufacture, characterisation and application of cellular metals and metal foams. Progress in Materials Science 46 (6):559-U553.

9. Medraj M, Baril E, Loya V, Lefebvre LP (2007) The effect of microstructure on the permeability of metallic foams. Journal of Materials Science 42 (12):4372-4383.

10. Baril E, Mostafid A, Lefebvre LP, Medraj M (2008) Experimental demonstration of entrance/exit effects on the permeability measurements of porous materials. Advanced Engineering Materials 10 (9):889-894.

11. Lefebvre LP, Banhart J, Dunand DC (2008) Porous metals and metallic foams: Current status and recent developments. Advanced Engineering Materials 10 (9):775-787.

12. Thelen S, Barthelat F, Brinson LC (2004) Mechanics considerations for microporous titanium as an orthopedic implant material. Journal of Biomedical Materials Research Part A 69A (4):601-610.

13. Zhang YH, Zhang YC, Tang HQ, Wang LH (2010) Images acquisition of a high-speed boring cutter for tool condition monitoring purposes. International Journal of Advanced Manufacturing Technology 48 (5-8):455-460.

14. Kerr D, Pengilley J, Garwood R (2006) Assessment and visualisation of machine tool wear using computer vision. International Journal of Advanced Manufacturing Technology 28 (7-8):781-791.

15. Wang W, Wong YS, Hong GS (2005) Flank wear measurement by successive image analysis. Computers in Industry 56 (8-9):816-830.

16. Wang WH, Hong GS, Wong YS (2006) Flank wear measurement by a threshold independent method with sub-pixel accuracy. International Journal of Machine Tools & Manufacture 46 (2):199-207.

17. Atli AV, Urhan O, Erturk S, Sonmez M (2006) A computer vision-based fast approach to drilling tool condition monitoring. Proceedings of the Institution of Mechanical Engineers Part B – Journal of Engineering Manufacture 220 (9):1409-1415.

18. Malcolm AA, Leong HY, Spowage AC, Shacklock AP (2007) Image segmentation and analysis for porosity measurement. Journal of Materials Processing Technology 192:391-396.

19. Prokop J, Sveda L, Jancarek A, Pina L (2009) Porosity measurement method by x-ray computed tomography. Fractography of Advanced Ceramics Iii 409:402-405.

20. Tutunea-Fatan OR, Abolghasemi Fakhri M, Bordatchev EV (2010) Porosity and Cutting Forces: From Macroscale to Microscale Machining Correlations, accepted for publication in Proceedings of the Institution of Mechanical Engineers Part B – Journal of Engineering Manufacture.

21. Lefebvre LP, Thomas Y (2003) Method of making open cell material, United States Patent No. 6660224.

22. Bendat JS, Piersol AG (1993) Engineering Applications of Correlation and Spectral Analysis, John Wiley & Sons, New York.

Chapter 4

4 Experimental Analysis of the Effect of Process Parameters during Micromilling of Porous Ti

4.1 Introduction

Titanium foam is a class of porous metallic materials produced through powder metallurgy. These materials found multiple applications in biomedical area owed to their excellent biocompatibility properties enabled by their macroscopic porosity, light weight and high strength. Regardless if used as standalone materials or as coatings on the surface of solid structures, titanium foams become in the recent years one of the most desirable materials in fabrication of orthopaedic and dental implants [1-3].

Although the end-products manufactured from titanium foams generally involve net-shape or near-net shape technologies, large fractions of them are subjected to secondary finish/machining operations before final use and assembly [4]. These secondary operations enable attaining of dimensional and surface finish parameters that cannot be obtained directly through sintering [5]. Also, there are numerous types of geometric features whose generation is practically impossible without the involvement of secondary machining operations. Under this category one can find often listed narrow slots, bevels, threads, blind holes, or other types of re-entrants normal to sintering direction. It is estimated that about half of the components produced through powder metallurgy require secondary machining operations [6].

The size of the components produced from titanium foams varies between large limits, but many of them, especially those intended for biomedical purposes tend to be relatively

small in size. As a result, micromachining technology represents one of the attractive solutions that can be used to meet the high quality constraints required by these products.

Although extensive research efforts have already been directed towards micromilling of solid metallic materials, little is known about the mechanics and dynamics of micromilling when applied on porous metallic foams. One of the most common topics in prior studies on micromilling is done by the development of accurate cutting force models [7-9]. However, the underlying assumption in all these works is that the material is characterized by continuous properties, which is not the case of porous foams. For these materials, porosity distribution affects the magnitude of the cutting forces in a direct manner that can be outlined by simply comparing cutting force signatures obtained while micromilling porous and continuous samples involving the same base material [10]. Moreover, the use of tools whose sizes are comparable with pore dimensions give rise to a whole new set of challenges related to process stability and cutter durability.

However, it is reasonable to expect that in addition to the aforementioned porosity distribution, the process parameters themselves play a role on the magnitude of the cutting forces. As a result, the current study aims to determine the relative order of priority in the balance between porosity and primary process parameters in their combined effect on the stability of the cutting process during micromilling of porous titanium foams. The influence of both porosity and micromilling parameters on cutting forces will be analyzed from a statistical perspective, by involving the use of appropriate statistical measures.

4.2 Factors Affecting Cutting Force Signature in Porous Micromilling

Titanium foams are characterized by a highly porous structure (Figure 4.1). Pores have variable sizes – typically ranging between 50 and 400 microns – random shapes and they have a non-uniform volumetric distribution. As a requirement imposed by biomedical applications, pores have to be open and form an interconnected network to facilitate the osteointegration process. When micromilling is performed with tools ranging from 0.2 to 0.8 mm diameter, their cutting edges experience frequent engagement with solid titanium material, but its duration and repeatability are low and hence relatively difficult to predict. This recurring contact between cutting tool and solid titanium constitute the primary cause of material removal operation and a number of theories have been proposed to describe it [10].
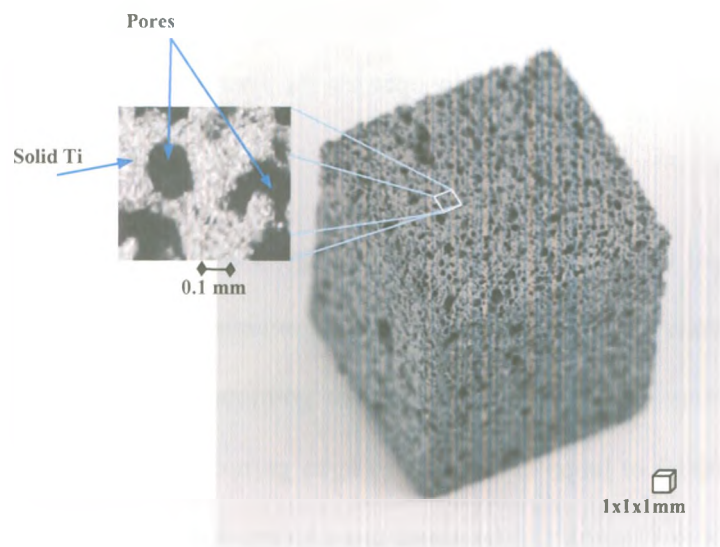
Figure 4-1: Sample of titanium foam outlining three-dimensional porosity

4.2.1   Porosity Distribution Along The Tool Path

Numerous models for cutting force prediction in micromilling of solid materials have been proposed [11-13]. Most of these models are formulated by assuming a predictable circular cutting edge trajectory as yielded from Martelotti's approximation of the real trochoidal curve [14]. Since analytical determinations of the volume of material removed in one tool revolution are possible, the magnitude of the cutting forces can be estimated with sufficient accuracy.

When micromilling is used in finishing operations performed on porous materials, the cutting edges of the tool are engaged only for a limited amount of time, such that many of the continuous cutting assumptions are no longer valid. Since in finish micromilling operations, pore profile does not change significantly with depth, the volume of material removed in each tool revolution can be estimated with an acceptable precision based on the amount of porosity determined at the top of the surface to be machined. Without losing the generality of the approach, all subsequent considerations will be made in the assumption of a two-flute cutter.

As shown in Figure 4-2a, the area swept during i-th tooth revolution (A_i) represents in fact the difference between the semicircular surfaces covered by two consecutive cutting edge trajectories T_{i-1} and T_i. According to cutting kinematics, the maximum distance between any pair of successive cutting edge trajectories is equal to feed/tooth value (f). No difference between the area swept (A_i) and removed (S_i) during i-th tooth revolution exists in micromilling of continuous materials (Figure 4-2b):

$$S_i = \int_0^\pi [R_{T_i}(\theta) - R_{T_{i-1}}(\theta)]d\theta = A_i \qquad (1)$$

where $R_{T_{i-1}}(\theta)$, $R_{T_i}(\theta)$ represent radial distances from points on T_{i-1}, T_i cutting trajectories respectively, and center of the i-th cutter revolution. The instantaneous location of the point on the cutting trajectory is identifiable through the value of the angular parameter θ.

Assuming that feed/tooth is constant during micromilling, the area swept between any pair of successive cutting edge trajectories will be identical along the entire tool path. As a result, the area (A_i) and volume (V_i) of material removed during each tooth revolution are constant for the entire micromilling operation.

By contrast, when micromilling is performed with identical process settings on porous foams, only pure geometric parameters, like A_i, preserve their values over the entire duration of the operation. The amount of material removed, whether measured in 2D (S_i) or in 3D (V_i) changes continuously for each new revolution of the tooth, since it is determined by the relative fraction between solid material and voids (pores) contained within A_i:

$$S_i = \sum_k \int_{\alpha_k}^{\alpha_{k+1}} [R_{T_i}(\theta) - R_{T_{i-1}}(\theta)]d\theta \leq A_i \quad (2)$$

where the area delimited by α_k, α_{k+1} angular parameters and T_{i-1}, T_i curves encompasses solid material only. The radii $R_{T_{i-1}}(\theta)$, $R_{T_i}(\theta)$ have the same meaning as in Equation (1). Obviously, the number of voids/pores existent in each area swept during individual cutter

revolution has a random variation along the tool path, since it is determined by the overall porosity of the titanium foam.

The proportion of solid material p_i in the area swept per tooth revolution can be quantified as:

$$p_i = \frac{S_i}{A_i} \qquad (3)$$

with $p_i \in [0, 1]$. Here, $p_i = 0$ corresponds to no material removal and $p_i = 1$ corresponds to solid material cut (no pores in A_i). Since instantaneous magnitudes of cutting forces in micromilling are proportional to the amount of material being removed in each cutter revolution, it can be inferred that for a porous material, cutting force signature correlates in fact with p_i. Representative samples of cutting force variations for continuous and porous titanium are illustrated in Figure 4-2c.
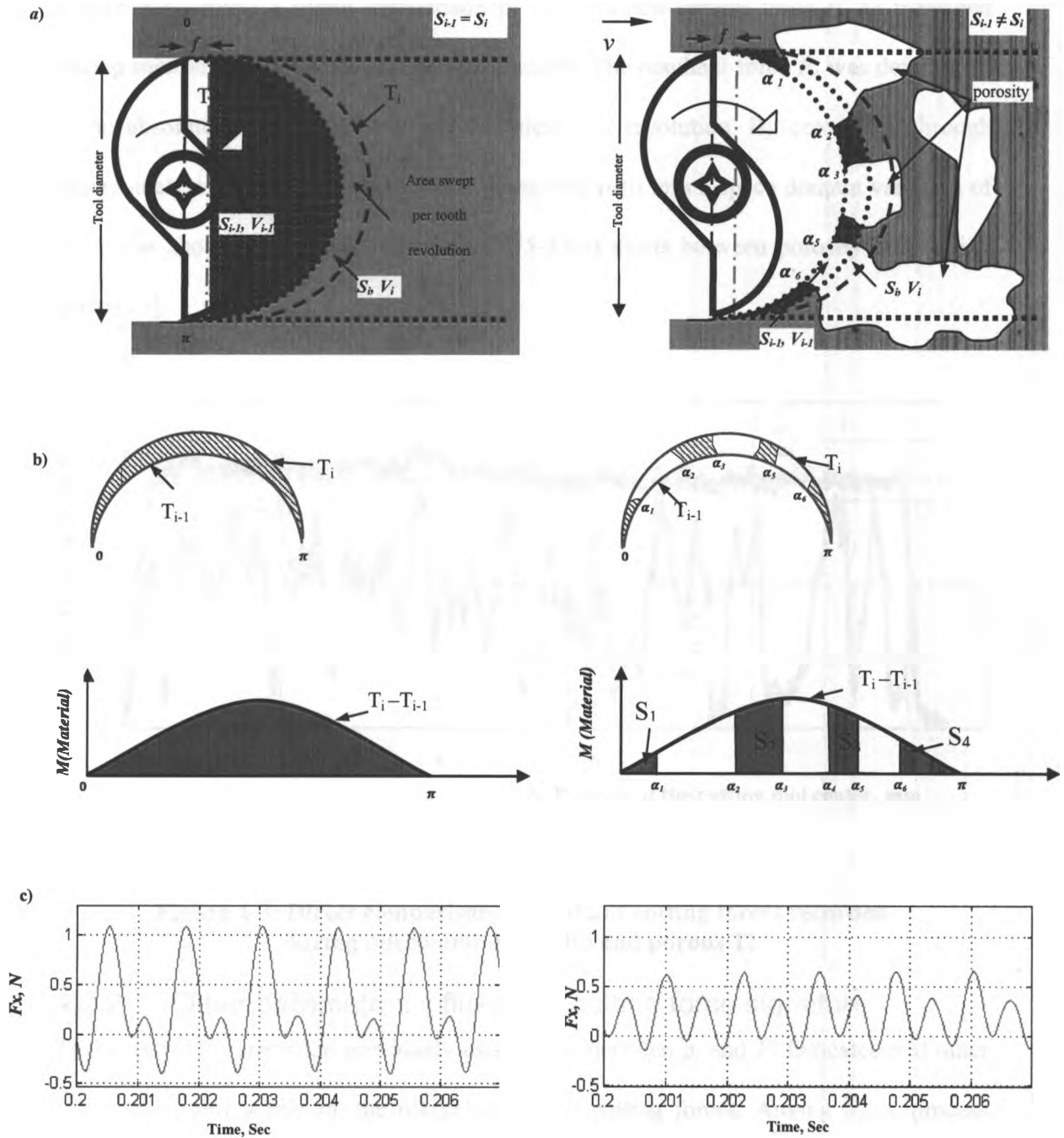
Figure 4-2: Comparisons between solid and porous titanium micromilling:
a) Kinematics of the cutting edges in micromilling;
b) Estimating the amount of material removed per tooth revolution; and
c) Cutting force signature in time domain.

Figure 4-3 depicts a direct comparison of the resultant cutting force F_r as measured during micromilling of solid and porous titanium. The resultant force F_r was determined as an absolute mean value over one complete tool revolution. By converting through image analysis the porosity distribution along tool path into a space domain variation of p_i, it was shown that a good correlation (75-85%) exists between porosity and cutting force [15].
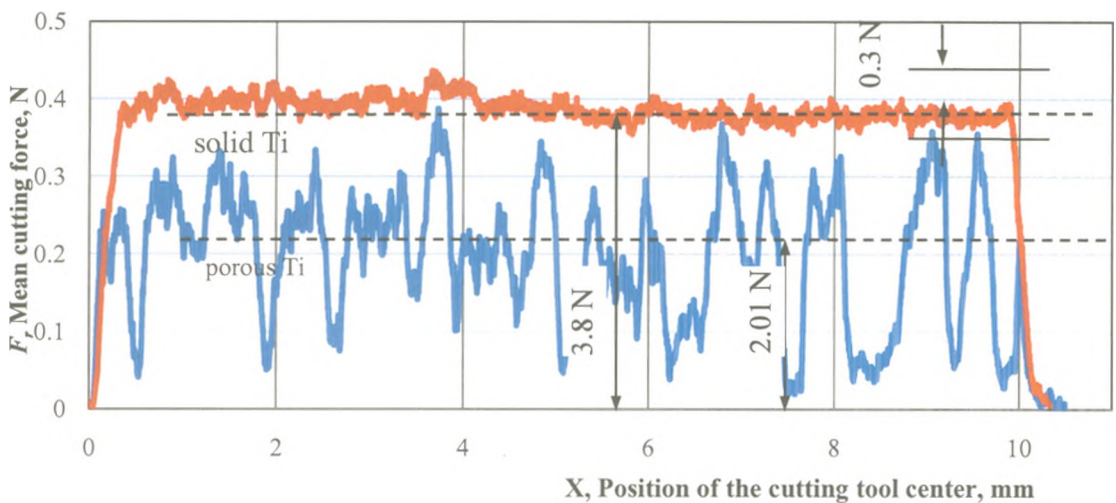
Figure 4-3: Direct comparison of resultant cutting forces recorded during micromilling of solid and porous Ti.

4.2.2   Other parameters influencing cutting force signature

The amount of correlation previously established between p_i and F_r indicates that other factors also play a role on the magnitude of the cutting forces. Among them, process parameters related to the dynamics of the micromilling process (cutting speed and feedrate) constitute an obvious choice, since their effect on the cutting forces experienced during machining of continuous materials is well known. In addition to process parameters, cutting force signature is strongly dependent on the accuracy of cutter

positioning within tool holder. In this sense, cutter runout is known to have an important effect on the magnitude of the cutting forces [7].

Similar to macroscale machining, micromilling is a process caused by the shearing of the material along the slipping planes induced by the cutting edges of the tool. When material has a homogeneous structure, shearing happens only along known and controlled directions within micromilled material, such that the two side edges of the microslot are always parallel to main feed direction imposed by machine tool stages. By contrast, in porous material micromilling, microslots are characterized by highly irregular side edges, especially in zones adjacent to large voids (Figure 4-4). This phenomenon is probably caused by an uncontrolled shearing of the material caused by a springback effect of the tool that tends to revert to its minimal energy (i.e. underformed) state when reaction force generated by the machined material is low. Under normal cutting conditions, tip of the cutter is deflected in an opposed to feed direction. The alternation of cutter engagement/disengagement conditions responsible for variable cutter deflections has an important effect on cutting force signature. Experimentally, the aforementioned springback effect is more pronounced for small-sized tools.
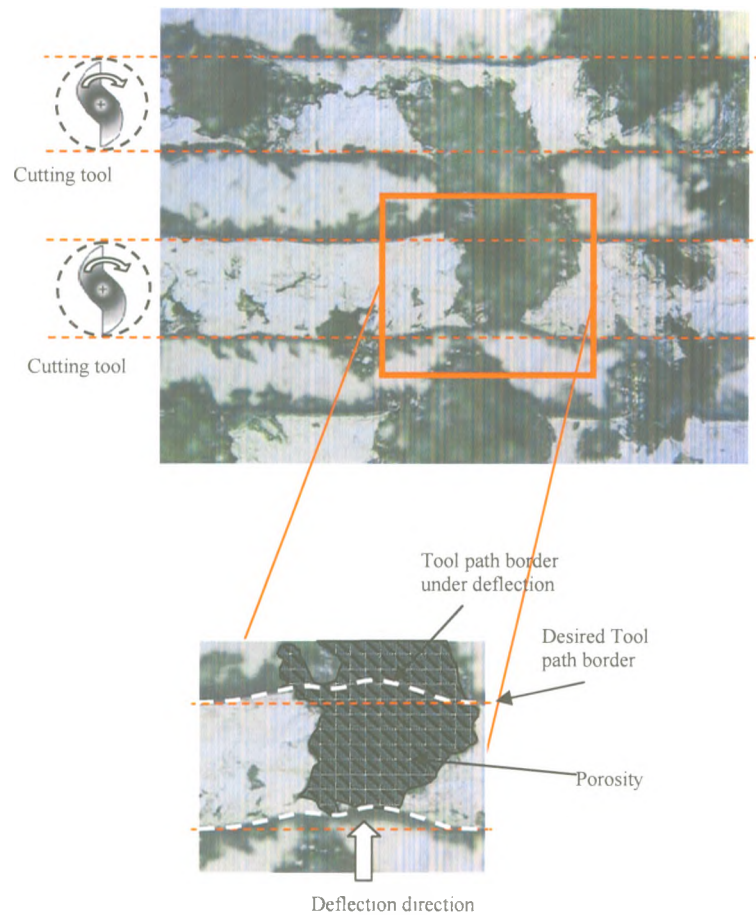
Figure 4-4: Tool path irregularities caused by large voids.

In porous titanium micromilling, shearing is not the only phenomenon responsible for material removal. A more in-depth analysis of the microstructural configuration of the material reveals that this material is actually comprised from a large number of interconnected porosities between which clusters of spherical particles of sintered titanium can be observed (Figure 4-5). As a result, material removal can also occur due to microparticle breakout/detachment, in which case cutting forces will deviate from their regular pattern of variation. Porous structure of the titanium foam is also responsible for

random changes in the magnitude of the cutting forces induced by sudden collapses of the

porous structure under cutting tool tip pressure (Figure 4-6).
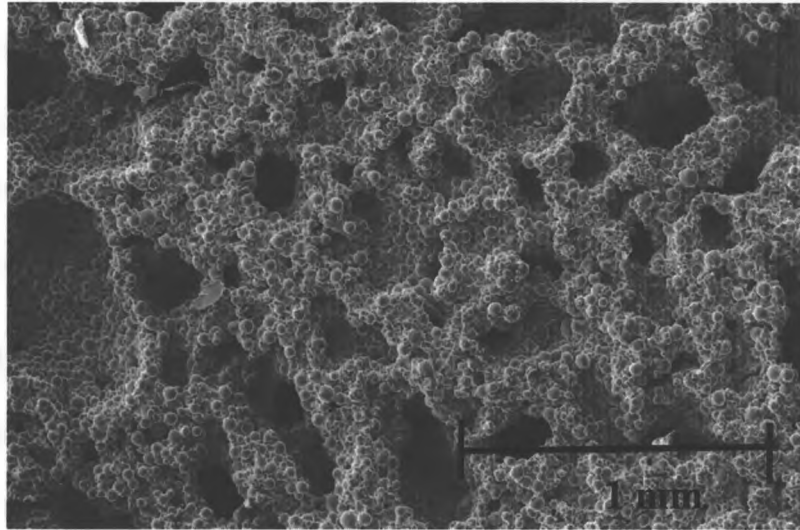
Figure 4-5: Microscopic view of Titanium foam composed of clusters of particles connected to each other in random conditions.
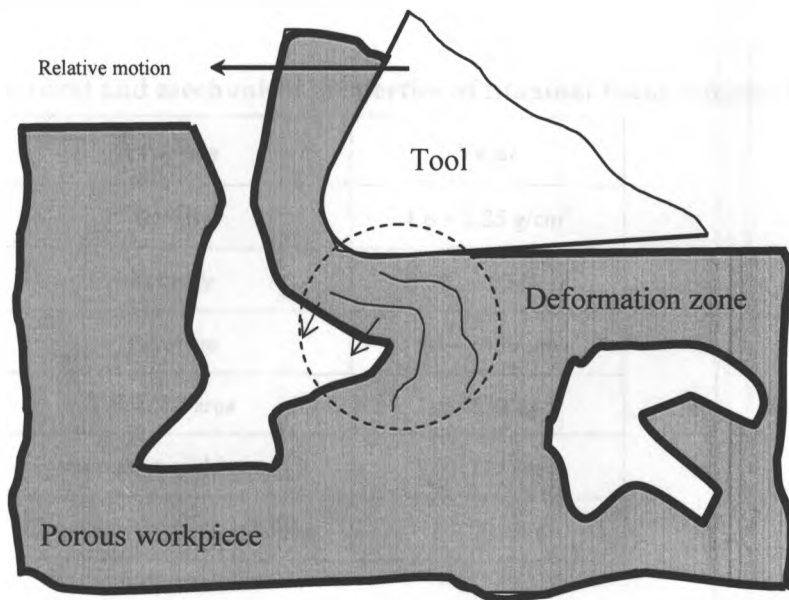
Figure 4-6: Porosity closures under cutting tool tip pressure.

4.3 Experimental Setup and Methodology

Experimental analysis was performed to study the effect of the different cutting parameters in micromilling of Ti foams. Real-time cutting forces and motions data measurements carried out during Micro-milling. Acquired data later used to calculate the resultant cutting force synchronized in spatial domain and compatible with porosity measurements. Later on, the statistical analysis performed to investigate the effect of different parameters in correlation of two data sets.

4.3.1 Material Used

Titanium foam samples used in this study were manufactured by the Industrial Material Institute of the National Research Council of Canada (Boucherville, Quebec) through a proprietary powder metallurgy procedure [16]. Structural and mechanical properties of the Ti foam are presented in Table 4-1. The samples had a cubic shape with an approximate side length of 13 mm (Figure 4-1).

Table 4-1: Structural and mechanical properties of titanium foam samples [3]

Property	Value
Density	$1.6 - 2.25$ g/cm^3
Porosity	$50 - 65$ %
Pore size	$50 - 1400$ µm
Surface area	0.05 m^2/g
Compressive yield strength	$25 - 125$ MPa
Compressive elastic modulus	$5 - 20$ GPa

4.3.2   Experimental Setup For Micromilling Experiments

A custom-built five-axis CNC micromilling system (Figure 4-7) was used to perform microslot cutting experiments. The system was equipped with an air-bearing spindle capable of rotational speeds between 5,000 and 100,000 rpm range. The micromilling system was characterized by a maximum travel range on X and Y axes of 300 mm and a static positional accuracy of 1 µm.

Cutting experiments were performed with two-flute, uncoated, tungsten carbide flat-end micromills with diameters varying between 200 and 400 microns. Their helix and clearance angles were 25° and 6°, respectively. The microslots cut were placed on the top face of cubic titanium foam samples and their geometry was defined by a constant length of 10 mm and depths varying between 5 and 15 microns. A total number of 6 experiments was performed. A detailed breakdown of their parameters is given in Table 4-2.
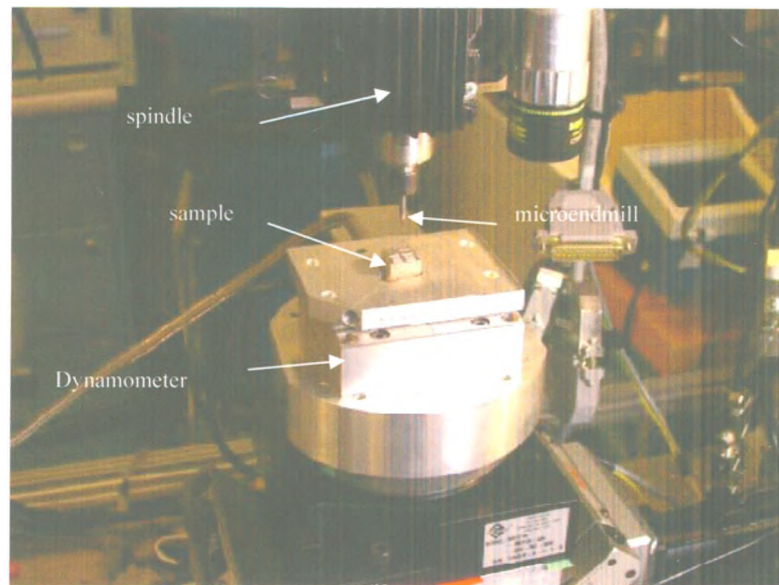
Figure 4-7: Experimental setup used for cutting force measurements
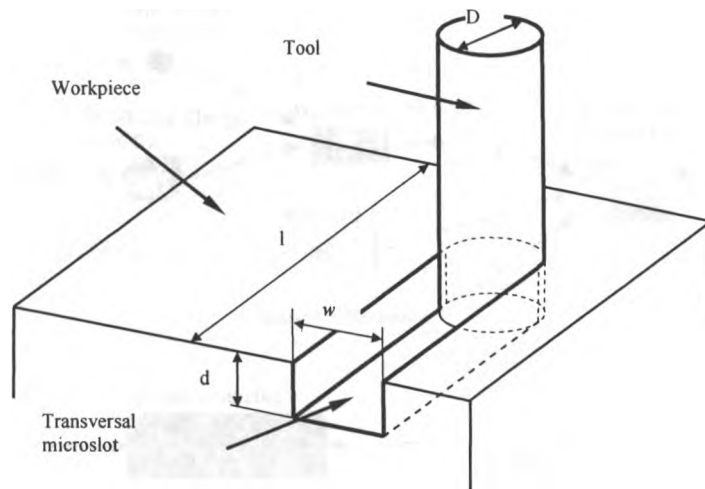
Figure 4-8: Geometric parameters of the microslot.

4.3.3   Cutting Force Measurements

An in-house developed data acquisition system for micromilling cutting force was used in this study (Figure 4-9). The three orthogonal cutting force components were measured with a Kistler dynamometer (type 9256C2) connected to a Kistler dual mode charge amplifier (type 5010B). The signals outputted by positional encoders connected to the three translational stages of the machine tool were measured in real-time along with the three-phase current consumed by the spindle drive. Cutting force components $F_X(t)$, $F_Y(t)$, $F_Z(t)$ and spindle current $I(t)$ were recorded in real-time with a sampling frequency of 25kHz and a minimum threshold of 0.002 N.
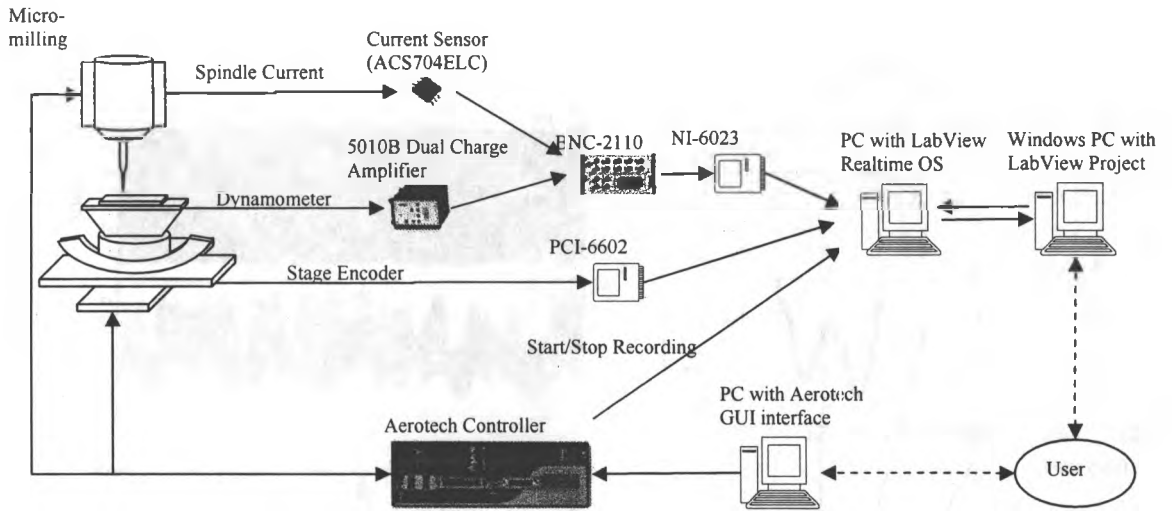
Figure 4-9: Cutting force data acquisition system.

4.3.4 Cutting Force Calculations

The raw values of the measured cutting forces were averaged over each cutter revolution. The beginning and end of each revolution was precisely determined based on the time variation of one phase of the spindle current (Figure 4-10). In addition to the measured F_X, F_Y, and F_Z components, a resultant cutting force was determined through vectorial summation of X and Y components of the cutting force ($\overline{\overline{F}}_R = \overline{\overline{F}}_X + \overline{\overline{F}}_Y$).
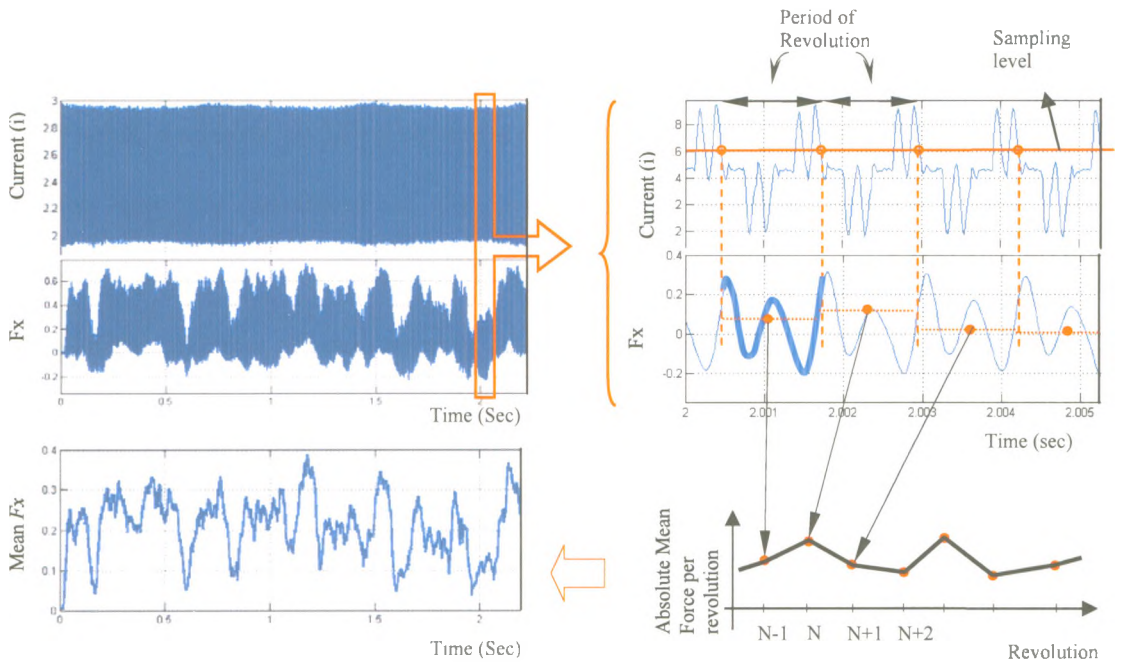
Figure 4-10: Calculation of the resultant cutting force.

4.3.5   Optical Determination of Porosity

A complete methodology for vision-based estimation of porosity in micromilling operations was introduced and discussed in detailin [15]. However, this study relied on a more accurate method of porosity determination based on optical micrographs captured with a Wyko interferometric microscope, rather than the conventional digital camera used in the prior study [15]. The images generated by the optical profilometer have a higher resolution and provide complete topographic chart of the analyzed surface. Since this study is focused on finish micromilling operations with depths of cut relatively small (< 15 µm), it was assumed that the voids do not have significant cross sectional variations in

horizontal *XY* plane. Because of this assumption, porosities measured on initial (unmachined) and machined surfaces are presumed as approximately equal.

In this work, a number 10 objective and a field of view of 0.5 mm was used to generate a 1.9 µm sampling resolution of the optical profile acquired by the system. The micrographs acquired with optical profilometer include different colors that are correlated with vertical location of each point of the analyzed surface (Figure 4-11a). The initial pictures were subsequently converted to grey (Figure 4-11b) and then binary images (Figure 4-11c) to clearly define porosity contour. The micrographs were optically thresholded by using Otsu 's method in such a way to ensure that surface indentations deeper than 3 µm were regarded as pores.
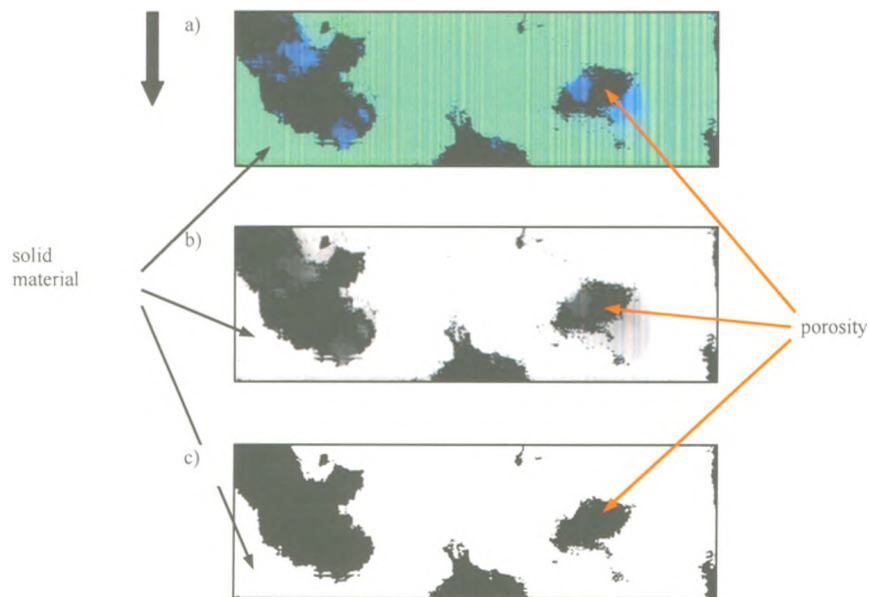
Figure 4-11: Digital conversions of optical micrographs:
a) original; b) grey scale; and c) binary.

In order to determine the proportion of solid material in the area swept per tooth revolution (Equation 3), the schematic showing cutting edge trajectories (Figure 4-2) was overlapped with binary map of the material surface obtained as a result of the aforementioned successive image conversions. The fraction between the "on" and total number of pixels enclosed between two consecutive cutting edge trajectories will allow determination of the space-dependent porosity profile along the analyzed tool path (Figure 4-12)
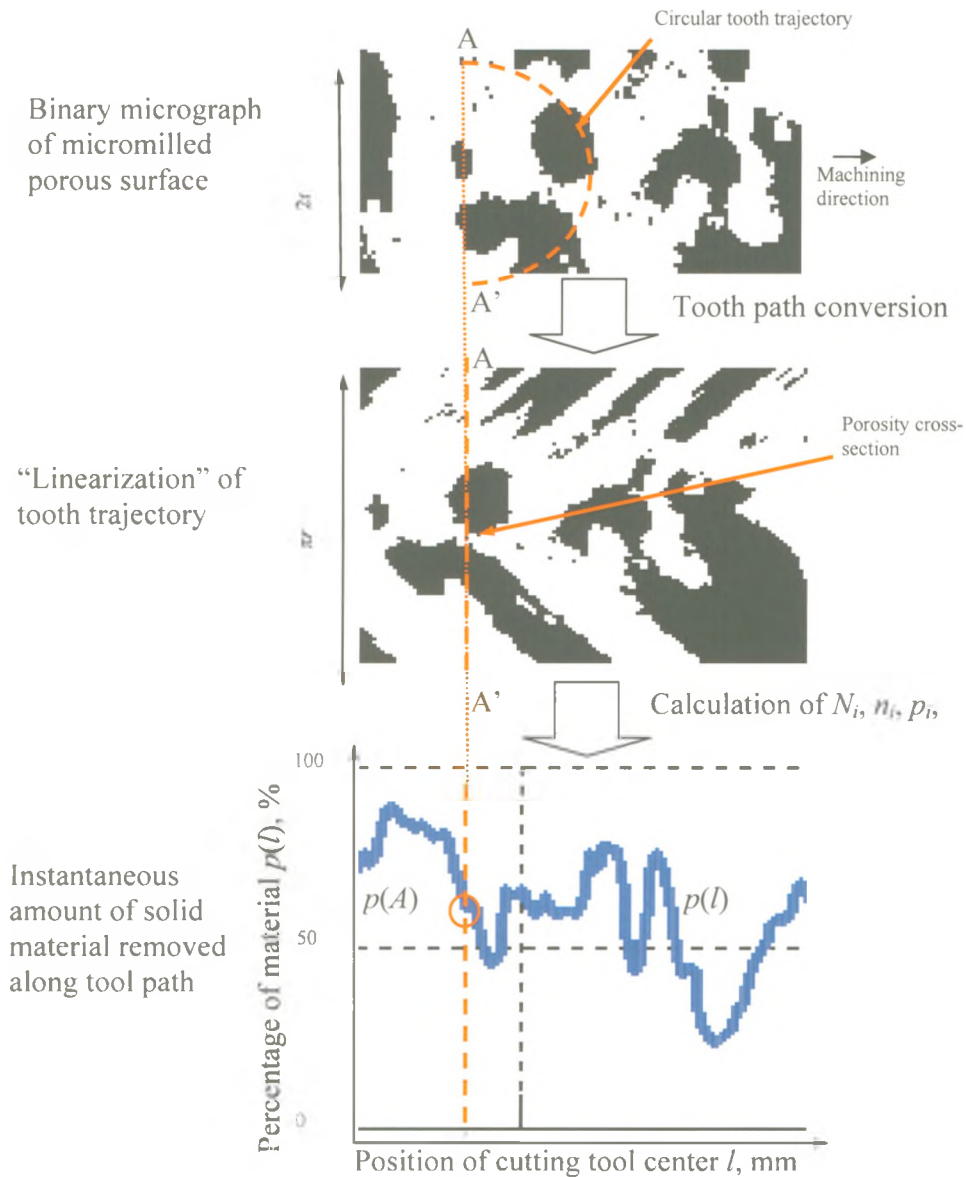
Figure 4-12: Space-dependent porosity assessment along tool path.

4.3.6   Porosity and cutting force correlations

Statistical analysis was carried out to investigate correlations between porosity and

cutting forces. This analysis was performed on two datasets: 1) solid material proportion

p (Section 4-3.5); and 2) resultant cutting force (Section 4.3.4). The required

synchronization between the two datasets was guaranteed by converting the original time-dependent cutting forces values $F(t)$ into space-dependent representations $F(l)$. The conversion was made possible due to the simultaneous recording of the linear tool position (l) with the system presented in Figure 4-9.
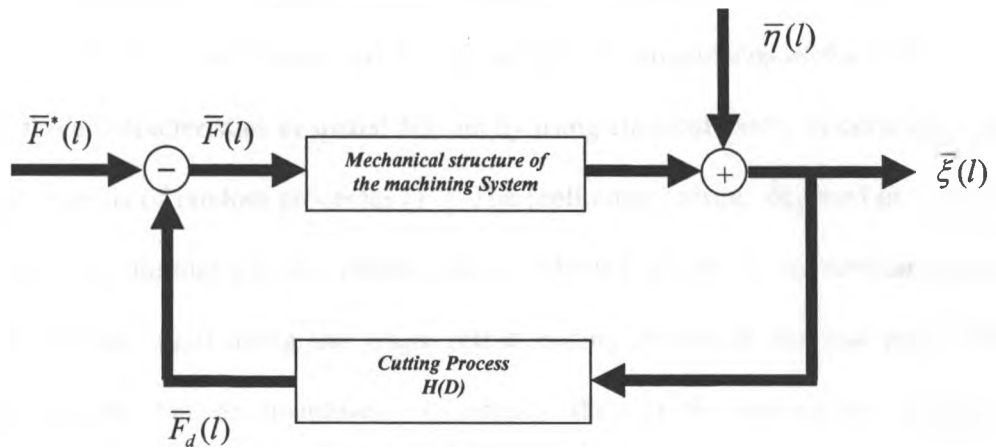
Figure 4-13: Block diagram outlining the effect of porosity on the overall dynamics of the cutting process

Based on the general dynamics of the machining system, a dynamic correlation links deflection of the tool $\xi(l)$ and cutting forces developed at cutter/workpiece contact interface $F(l)$ (Figure 4-13). The presence of voids within porous material changes the size of contact between tool and workpiece and in turn affects cutting forces developed at their common interface. Because of this, it can be inferred that a closed loop dynamic relation exists between cutting forces and cutter deflection:

$$\begin{cases} \bar{\xi}(l) = W(d)\bar{F}(l) + \bar{\eta}(l) \\ \bar{F}(l) = H(D)\bar{\xi}(l) + \bar{F}^*(l) \end{cases} \quad (4)$$

where $\eta(l)$ represents dynamic porosity contribution, $W(d)$ is the dynamic operator of the mechanical structure of the machining system, $H(D)$ is the dynamic operator of the cutting process, $\overline{F}^*(l)$ Mean value of cutting forces, $\overline{F}_d(l)$ force component generated by cutting process variation and $D=d/dt$ is the differential operator.

The goal of this study is determination of statistical correlations between porosity and cutting forces. This can be achieved through statistical comparisons of the porosity and cutting force characteristics in spatial domain by using classical theory of correlation and spectral analysis of random processes [17]. The preliminary results depicted in Figure 4-14 clearly indicate that porosity pattern $p(l)$ is followed closely by the resultant cutting force magnitude $F_R(l)$ along the entire stable cutting region of the tool path. Their interdependence can be quantified numerically through the correlation coefficient expressed in its normalized form for two discrete random signals α and β as:

$$C = \frac{\sigma_{\alpha\beta}}{\sigma_\alpha \sigma_\beta} \quad (5)$$

$$\sigma_{xy} = \lim_{N \to \infty} \frac{1}{N} \sum_{i=1}^{N} (x_i - \mu_x)(y_i - \mu_y) \quad (6)$$

where σ constitutes standard deviation. The correlation coefficient indicates how well one variable can be predicted from the other. Another statistical metric with significant practical implications is represented by the power spectral density (PSD) that can be used as an indicator of the frequencies at which variations of the two analyzed signals are strong (or weak). A better match between PSDs of the two signals generally implies a good interdependence between them. To further assess their interplay numerically, a

common statistical metric used is coherence function. Elevated mean coherence function values (> 0.70) are generally regarded as good indicators of the fact that the output that is produced by the analyzed input over frequency domains where coherence function is characterized by high values. All these statistical measures are implemented as standard Matlab functions.
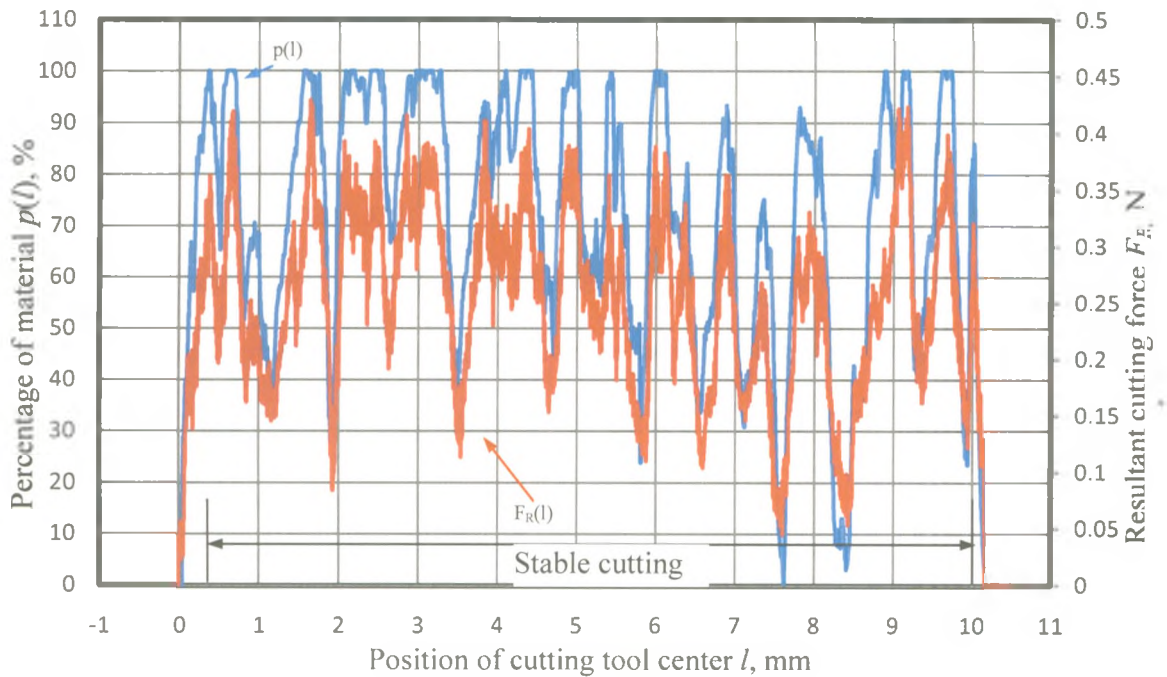
Figure 4-14: Comparison between the amount of solid material removed p and resultant cutting force F_R

As Figure 4-14 shows, the agreement between the porosity and cutting force signals is not 100%, since a certain component of the cutting force is still determined by conventional cutting process parameters. Thus, the total cutting force generated during porous material micromilling can be represented as a sum of two components:

$$\overline{F}(l) = \overline{F}_c(l) + \overline{F}_p(l) \qquad (7)$$

Where $\overline{F}(l)$ is the total cutting force, $\overline{F}_c(l)$ is the component determined by the cutting process itself (cutter/workpiece interactions), and $\overline{F}_p(l)$ is the component of the cutting force influenced by the porosity. As expected, the use of statistical measures, like correlation coefficient, is unable to estimate the effect brought by each individual cutting force component ($\overline{F}_c(l)$ and $\overline{F}_p(l)$). However, correlation coefficient constitutes a good first estimation of the statistical interplay between cutting force and porosity or, in other words, the volume of material removed.

In order to detail further the statistical structure of the correlation between porosity and cutting forces, analysis and comparison of spatial frequency characteristics of porosity and cutting force, e.g. power spectrum densities in spatial frequency domain, is required. In addition, the use of a coherence function will allow estimation of the individual effect of $\overline{F}_c(l)$ and $\overline{F}_p(l)$ on total cutting force.

4.4   Effect of Process Parameters on Porosity-Cutting Force Correlation

As mentioned, in porous material micromilling, cutting force fluctuations can be correlated not only with the proportion of solid material within the area swept by cutting edges, but also with cutting parameters like: spindle speed, chip load (feed rate), tool size, and cutting depth. Their effect generally translates into a bidirectional (i.e. superior or inferior) correlation between cutting forces and porosity pattern.

A set of experiments (Table 2) has been devised to investigate the individual effect of variable micromilling parameters on primary porosity-cutting force correlation that was

quantified through statistical measures. This matrix of experiments allows paired comparisons between experiments with singular modifications in terms of cutting parameters used. To exemplify, the only change made between experiments E2 and E6 is spindle speed, between E5 and E6 is chip load (feed rate), between E1 and E6 is tool diameter, and between E3 and E4 is cutting depth. As a result, these specific pairs of experiments will be analyzed and compared further in Sections 4.4.1 through 4.4.

Table 4-2: Matrix of experimental micromilling parameters used

	Cutting speed (m/s)	Feed rate	RPM	Depth of cut(μm)	Chip load (μm)
E1	0.5	95.54	47771	15	1
E2	0.5	95.54	23885	15	2
E3	0.5	47.77	23885	15	1
E4	0.5	47.77	23885	5	1
E5	1	191.08	47771	15	2
E6	1	95.54	47771	15	1

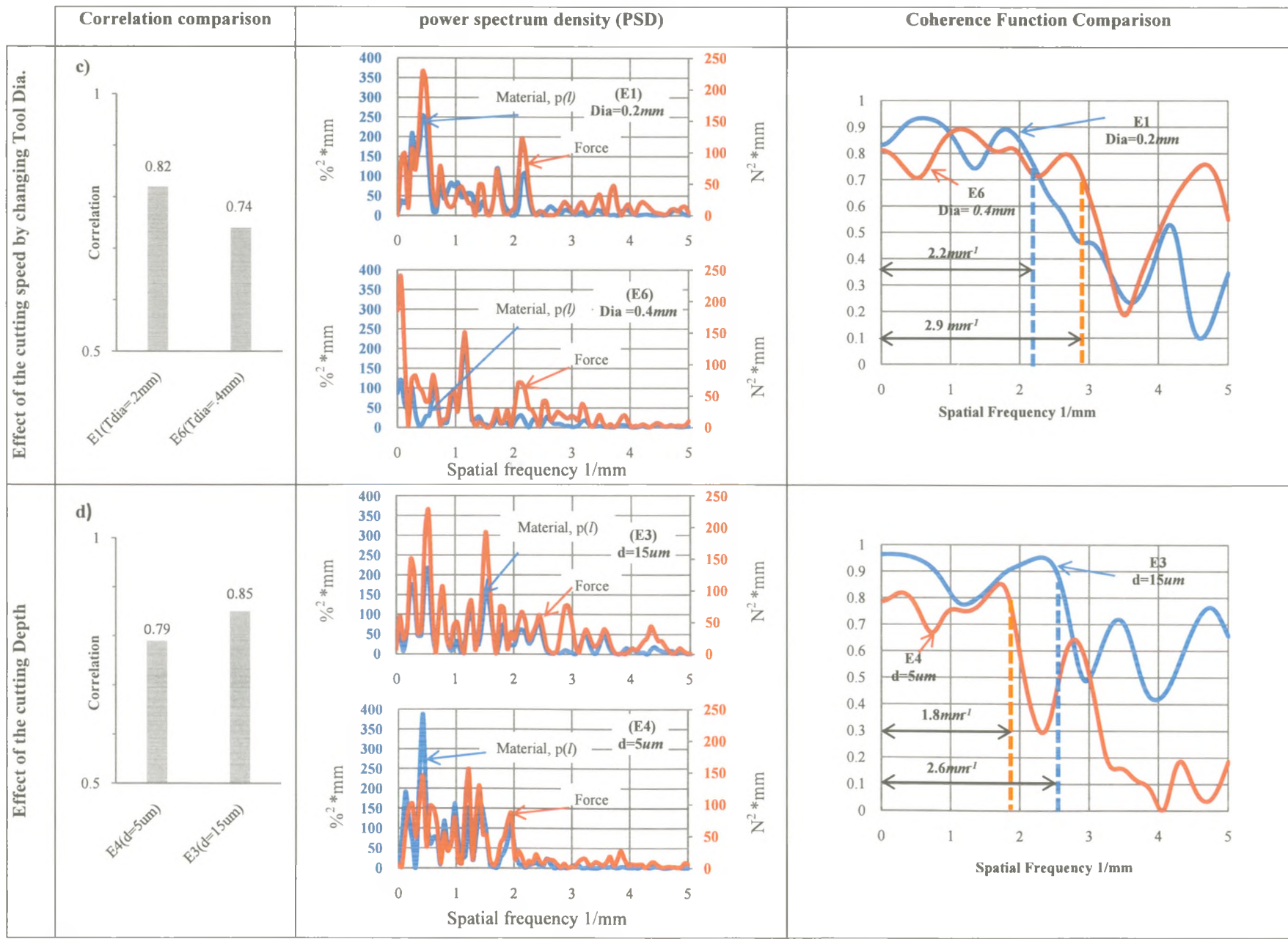| Correlation comparison | power spectrum density (PSD) | Coherence Function Comparison |
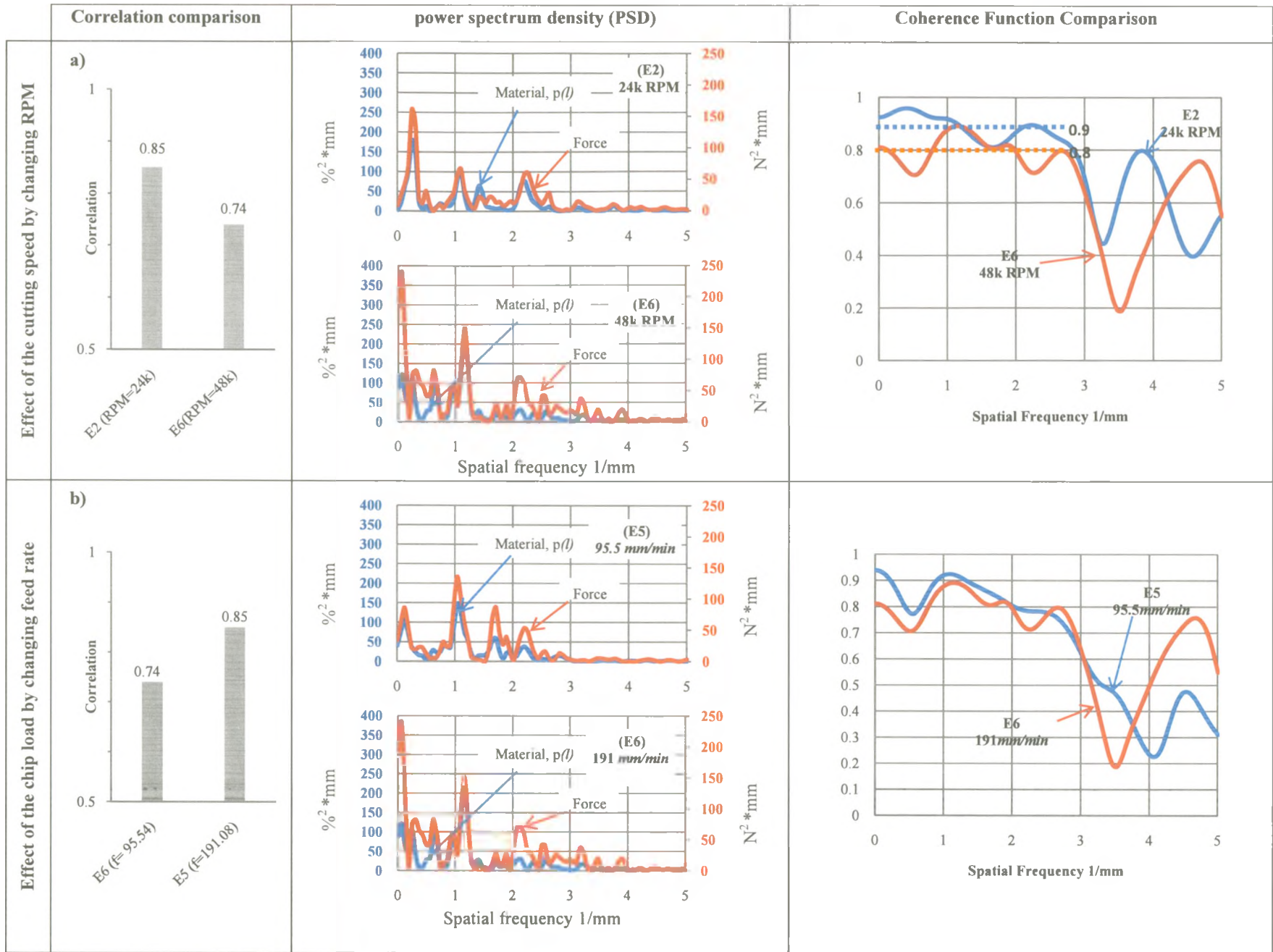
Figure 4-15: Effect of primary cutting parameters on correlation between porosity and resultant cutting force

4.4.1 Spindle Speed

As Figure 4-15a indicates, doubling up the spindle speed decreases significantly the correlation between porosity and cutting force, from 0.85 for 24,000 rpm to 0.75 for 48,000 rpm (13% reduction). This reduction could be explained through an increased effect of the mechanical shocks developed at cutter/workpiece interface, which interfere with primary porosity-cutting force correlation. According to a known machining theorem, spindle and cutting speed are in a relationship of direct proportionality.

The frequency component of both cutting force and porosity are similar, which explains the elevated level of the coherence function which is above a 0.8 threshold when analyzed within a frequency range of up to 2.8 mm^{-1}. This actually means that in lower frequency domain bandwidth, more than 80% of the cutting force is determined by the porosity distribution. Since for this frequency domain, the average coherence function is around 0.90, any significant increases (double up) in cutting speed causes significant changes in the signature of the cutting force power spectrum density (PSD). As a result, the mean value of coherence function for double cutting speeds drops by 11% to 0.80, and this indicates that the dependence between porosity and cutting force declines for higher cutting speeds.

4.4.2 Chip Load

In machining, a relationship of direct proportionality links feed rate and chip load. As such, a two fold increase in the feed rate from 95.54 mm/min to 191.08 mm/min translates into a double chip load changing from 1 μm/tooth to 2 μm/tooth. Micromilling kinematics (Figure 4-2), seem to suggest that chip load augmentation means an increased

interface (swept area) between cutter and workpiece, which in turn should translate into a more pronounced effect of the porosity on the cutting force.

As Figure 4-15b confirms, doubling up the feed rate translates into a correlation coefficient that increases from 0.74 to 0.85. Since PSD of the cutting force becomes closer to that of the porosity and coherence value goes up after the increase in feed rate, it can be assumed that micromilling processes with higher chip loads are more dependent on porosity.

4.4.3 Tool Diameter

According to general machining theorems, tool diameter exerts on the cutting speed an effect that is absolutely similar to that of the spindle speed. Small-sized tools are more deformable and therefore more sensitive to porosity.

As Figure 4-15c indicates, a double-sized tool (0.4 mm tool diameter in experiment E6 vs. 0.2 mm in experiment E1) reduced the correlation coefficient from 0.74 to 0.82. Moreover, a good match between PSDs of porosity and cutting force can be noticed for small-sized tool, especially in low spatial frequency domain. However, it is important to note that the frequency range where porosity is the main factor contributing to cutting force signature tends to be smaller for small-sized tools than for the larger ones (2.2 mm^{-1} compared to 2.9 mm^{-1}) although in terms of mean coherence function it still behaves better (0.85 compared to 0.79). It is important to emphasize that these results reiterate the conclusion of Section 4.4.1: higher cutting speeds, regardless if produced by higher tool diameters or higher spindle speeds tend to reduce the correlation between porosity and cutting force.

4.4.4   Cutting depth

Intuitively, when cutting depth in increased, the influence of the porosity should become more pronounced, since it affects to a larger extent the contact interface between cutter and workpiece.

Indeed, the results presented in Figure 4-15d point out that when cutting depth increases from 5 to 15 μm, the correlation coefficient between porosity and cutting force increases from 0.79 to 0.85. For deeper cuts, the contact between tool and workpiece increases, and hence the difference between porosity and cutting force PSDs becomes visually negligible. Even more than this, the frequency domain of coherence widens for deeper cuts from 1.8 mm^{-1} to 2.6 mm^{-1}, which suggests that the porosity is the main factor impacting the cutting force profile. A good average coherence function is associated with deeper cuts when compared to more superficial ones (0.89 vs. 0.77). These results echo appropriately the conclusion of Section 4.4.2: better correlations between porosity and cutting forces are obtained for larger contact zones between tool and workpiece.

4.5   Conclusions

This study investigated the effect of several primary cutting parameters on the correlation between porosity and cutting force as measured during titanium foam micromilling. The results obtained by comparing several statistical indicators seem to suggest that porosity has a major contribution on the cutting force signature profile in case of: i) less intensive cutting regimes; and ii) larger contact zones between cutter and workpiece. Both options outlined tend to increase the stability of the micromilling process when applied on porous

foams. Based on these conclusions, it can be speculated that continuity of the material will impact the amount of cutting force generated at cutter/workpiece interface only in case of less dynamic (slower) cutting processes, that practically allow the machining system to react to the changes in material structure/homogeneity. However, further research in this direction is required to support this hypothesis.

4.6 References

1. Baril E, Lefebvre L-P, Thomas Y, Ilinca F (2008) Foam-coated mim gives new edge to titanium implants. Metal Powder Report 63 (8):46-50.

2. Ryan G, Pandit A, Apatsidis DP (2006) Fabrication methods of porous metals for use in orthopaedic applications. Biomaterials 27 (13):2651-2670.

3. Banhart J, Weaire D (2002) On the road again: Metal foams find favor. Physics Today 55 (7):37-42.

4. Smith GT (1998) Getting the measure of pm machinability. Metal Powder Report 53 (5):31-35.

5. Eisenmann M (2000) Porous P/M Technology, ASM Handbook, vol. 7.

6. Alizadeh E (2008) Factors influencing the machinability of sintered steels. Powder Metallurgy and Metal Ceramics 47 (5-6):304-315.

7. P´erez H, Viz´an A (2007) Estimation of cutting forces in micromilling through the determination of specific cutting pressure. Materials Processing Technology 190 18–22

8. Engin S, Altintas Y. Generalized modelling of milling mechanics and dynamics: part I and part II—University of British Columbia. Department of Mechanical Engineering.

9. Bao W.Y, Tansel I.N, (2000) Modelling micro-end-milling operations. Part I and part II., Int. J. Mach. Tools Manuf. 40 2155–2192.

10. Tutunea-Fatan OR, Abolghasemi Fakhri M, Bordatchev EV (2010) Porosity and Cutting Forces: From Macroscale to Microscale Machining Correlations, accepted for publication in Proceedings of the Institution of Mechanical Engineers Part B – Journal of Engineering Manufacture.

11. Bao W.Y, Tansel I.N, (2000) Modelling micro-end-milling operations. Part I and part II., Int. J. Mach. Tools Manuf. 40 2155–2192.

12. Sutherland J.W, DeVor R.E, (1986) An improved method for cutting force and surface error prediction in flexible end milling systems, J. Eng. Ind. 108 269–279, Nov.

13. Kline W.A, DeVor R.E, (1983) The effect of run-out on cutting geometry and forces in end milling, Int. J. Mach. Tool Design Res. 23 (2/3) 123–140.

14. M. E. Martelotti, "Analysis of the Milling Process," Transactions of the ASME, vol. 67, p. 233, 1945.

15. A. Fakhri M, Bordatchev EV, Tutunea-Fatan OR (2010) Optical-based image analysis of porosity in micromilling of titanium foams, submitted to International Journal of Advanced Manufacturing Technology

16. Lefebvre LP, Thomas Y (2003) Method of making open cell material, United States Patent No. 6660224.

17. Bendat JS, Piersol AG (1993) Engineering Applications of Correlation and Spectral Analysis, John Wiley & Sons, New York.

5   Conclusions

The major goal of this study was to develop knowledge on the correlation between porosity and cutting forces as experienced during porous titanium foam micromilling. The work performed to accomplish this goal had a predominantly experimental nature and involved the development of an original image-based methodology required to assess the inherent porosity of the material as perceived by the cutting edges of the tool in their trochoidal motion along the intended tool path.

As outlined in Chapter 2, the prevailing mechanisms responsible for mechanics of porous material cutting are still largely unknown. The two theories previously proposed with this type of macroscale machining operations, namely interrupted cutting and deformation theory, seem to support only to a certain extent the experimental observations acquired in microscale domain. This seems to indicate that further challenges are introduced in processes in which the size of the tool is comparable to the size of the voids.

Statistical analysis used to investigate porosity-cutting forces correlations along with the effect exerted by primary cutting parameters on this correlation revealed three unique aspects of this interdependence:

1)   Higher correlation exists between them in low frequency domain when compare to high frequencies. When the distance between porosities becomes small, it is reasonable to expect that frequent excitations transmitted to the micromilling system will force it into a highly vibratory behavior that will simply overcome the regular interplay between cutting forces and material continuity.

2)   A superior correlation exists in less intensive cutting regimes, typically expressed through smaller cutting feeds. This observation echoes appropriately the first observation, since at smaller cutting feeds, the frequency of excitations decreases and hence material homogeneity becomes the primary factor with impact on cutting force signature.

3)   A superior correlation exists for larger tool/workpiece contact interfaces. As expected, once the magnitude of contact between the two main components of the cutting system increases, contribution of the material on cutting forces goes up, which in turn triggers corresponding decreases in the influence of the cutting process dynamics.

The overall conclusion of this work is that mechanics of the porous materials micromilling is ultimately controlled by the interplay between material continuity and dynamics of the cutting. Under appropriate conditions, any of these two components can become the predominant factor and therefore determine a particular behavior of the micromilling system.

Rational extensions of this work could aim to determine optimal process parameters that are capable to satisfy a desirable objective. Specific objectives with practical relevance are: acquiring of a controlled surface roughness or surface smearing, enhanced tool durability, reduced tool chatter, etc. Also, an interesting future research direction would involve development of an appropriate modeling of the process, based on coupled theoretical, numerical and experimental validations.